A model for H3K27me3 dynamics for the temporal control of transcriptional activation during flower development

Pelayo, Margaret Anne

Nara Institute of Science and Technology

Graduate School of Science and Technology

Laboratory of Plant Stem Cell Regulation and Floral Patterning

(Division of Biological Science)

(Professor Toshiro Ito)

Submitted on 2021 July 26

Laboratory (Supervisor)	Professor Toshiro Ito		
Name	Margaret Anne Pelayo	Date	2021 July 26
Title	A model for H3K27me3 dynamics for the temporal control of transcriptional activation during flower development		

During flower development, specialized stem cell niches called floral meristems (FM) localized at the tips of plant shoots will give rise to a pre-determined set of floral organs. The determinate nature of the FM is essential for proper flower formation and relies on FM termination. Proper timing of FM termination is important for proper organ formation and is regulated by the MADS domain transcription factor AGAMOUS (AG). FM termination regulated by AG involves the epigenetic activation of the C2H2-type zinc finger protein KNUCKLES (KNU) through passive H3K27me3 dilution along the *KNU* coding sequence in a cell cycle-dependent manner. However, how many other genes are similarly regulated remains unknown and the factors controlling this intrinsic timing mechanism (hereinafter referred to as 'biotimer'), especially at the chromatin level, have yet to be explored. Here, a general biotimer model is defined by the interplay between AG and PRC2 regulation, H3K27me3 status, and the cell cycle. Candidate biotimer genes were found through *in silico* analysis and the mechanistic components of the biotimer were examined through manipulation of histone modification at the *KNU* coding region. This chromatin-modified *KNU* line, named *6del*, was generated by iterative addition of an H3K27me-enriched and FIE-bound region from *KNU*'s coding sequence, and was demonstrated to delay *KNU*'s transcriptional activation and reduce *KNU* expression. Additionally, this effect was found to be PRC2- and cell cycle-dependent when *6del* is brought into PRC2 and cell cycle mutant backgrounds. These results suggest that PRC2 and the cell cycle regulate H3K27me3 accumulation and dilution on the extended *KNU* coding sequence in *6del*, respectively. Overall, these findings indicate an intrinsic temporal mechanism for proper transcriptional activation in floral stem cells during flower development.

Table of Contents

List of Figures and Tables

Figures

Tables

I. Introduction

Plants are sessile organisms that have the remarkable ability to continuously produce new organs throughout their life. For this continuous organogenesis, groups of undifferentiated cells called meristems play their key roles. Meristems are dynamically regulated to maintain the balance between cell proliferation and differentiation[1]. In *Arabidopsis*, floral meristems form a fixed number of floral organs[2]. At earlier stages, floral meristems keep producing enough cells by proliferation. At later stages of floral meristem growth, the balance shifts towards cell differentiation to terminate cell proliferation activity irreversibly[3–5]. Proper timing of this developmental shift called floral meristem termination enable plants to have a fixed number of floral organs.

The central regulator of floral meristem termination is the MADS domain transcription factor AGAMOUS (AG) [6–9]. AG represses *WUSCHEL* (*WUS*), which regulates the maintenance of stem cell populations in floral meristems. AG (as a tetramer with SEPALLATA (SEP) proteins) can directly and indirectly repress *WUS* (Fig. 1). AG directly represses *WUS* by mediating PRC2 recruitment on *WUS*[2]. Indirect pathways for *WUS* repression by AG involve two AG downstream targets, namely the YABBY transcription factor *CRABS CLAW* (*CRC*) and the C2H2-type zinc finger protein *KNUCKLES* (*KNU*). Recent work elucidated the networks involving CRC which was demonstrated to regulate auxin homeostasis for proper FM termination and gynoecium formation through its targets *TORNADO2* (*TRN2*) and *YUCCA4* (*YUC4*), a putative auxin transporter from the tetraspanin transmembrane protein family and an auxin biosynthesis gene, respectively[10,11]. AG also activates *KNUCKLES* (*KNU*) which encodes a repressor containing C2H2-type zinc finger protein, thereby

indirectly repressing *WUS* expression[2,10,12–16] (Fig. 1). A remarkable feature of *KNU* transcriptional activation is the observed two-day delay in its expression after AG recruitment to the *KNU* promoter region[13] (Fig. 1 and 2). At stage 2 of flower development, *KNU* expression is initially repressed by PRC2 bound at the *KNU* locus, which establishes and maintains repressive trimethylation at lysine 27 of histone H3 (H3K27me3) along its coding sequence[13,14,17]. By floral stage 3, AG protein is accumulated and displaces PRC2 from the *KNU* locus. PRC2-mediated H3K27me3 deposition is reduced and the subsequent decrease in H3K27me3 levels at the *KNU* locus occurs in a cell cycle-dependent manner. *KNU* is activated after two days of cell division cycles just before floral meristem termination[14]. This intrinsic timing mechanism (hereinafter referred to as "biotimer") under AG regulation is essential for proper flower development as altering *KNU* temporal expression has been shown to result in either premature floral meristem termination or in its indeterminacy[13]. AG has approximately 2000 target genes wherein *KNU* is currently the only known gene regulated by the AG biotimer mechanism[18]. Examples of AG targets associated with flower development and with regulatory roles are genes such as *STYLISH1* (*STY1*) for proper carpel development by regulating auxin biosynthesis, *INDETERMINATE DOMAIN 12* (*IDD12*) which belongs to the INDETERMINATE DOMAIN class of transcription factors (TFs) associated with gibberellic acid synthesis and response, *AT HOOK MOTIF NUCLEAR LOCALIZED PROTEIN* (*AHL18*) as a recently characterized modulator of root system architecture and *PLATZ10* (*PZ10*) a member of the novel TF class plant-specific zinc-dependent DNA-binding proteins[19–22]. However, how these genes are regulated by AG remains largely unknown.

PRC2 and other polycomb group (PcG) proteins establish repressive H3K27me3 marks at target genes resulting in transient and heritable gene silencing by chromatin compaction[23,24]. In this case, H3K27me3 is heritable throughout cell division and yet is also dynamic in response to intracellular and extracellular cues[25]. In plants, PRC2 regulates developmental transitions and cell type specification[26,27]. *Arabidopsis* PRC2 is known to have variant forms which determine the functions they exert over a particular developmental phase[26–29]. For example, flower development is largely associated with the EMF2-PRC2 variant made up of CURLY LEAF (CLF)/SWINGER (SWN), EMBRYONIC FLOWER 2 (EMF2), FERTILIZATION-INDEPENDENT ENDOSPERM (FIE), and MULTICOPY SUPPRESSOR OF IRA 1 (MSI1)[27]. Although characterization of PRC2 function has been described in detail, questions regarding how it drives proper temporal transitions during development remain. Various models have been postulated over the stable propagation of H3K27me3 over generations, as well as in its removal for activating gene expression[30–32]. Modes of chromatin reprogramming upon H3K27me3 removal can be actively controlled through histone demethylases, as well as passively when PRC2 is inactive at target loci[33]. *KNU* transcriptional activation relies on the passive mode of H3K27me3 removal which integrates cell division cycles resulting in the proper timing of *KNU* expression and essentially, of floral meristem termination[14].

The transition from indeterminacy to determinacy for FM cells signals the onset of cell differentiation upon termination of cell proliferation suggesting that FM cells become committed to a differentiation pathway during this transition[34]. Cell differentiation programs are tightly linked with the cell cycle

wherein cell cycle regulation is crucial for actively dividing cells to transition into differentiating cells leading to proper tissue and organ formation[35]. Progression through the cell cycle is driven mainly by the by the interaction of cyclin proteins (CYCs) and cyclin-dependent kinases (CDKs), a class of Ser/Thr kinases[36]. CYCs and CDKs form complexes which carry out the phosphorylation of various proteins involved in the progression of each cell cycle phase namely, G_1 (gap 1), S (synthesis), G_2 (gap 2), and M (mitosis). Among CDKs, B-type CDKs (CDKBs) are plant-specific CDKs and are considered associated solely with cell cycle regulation[36]. CDKBs consist of two subgroups, CDKB1 and CDKB2; and each subgroup has two members. CDKB1;1 and CDKB1;2 belong to CDKB1 while CDKB2;1 and CDKB2;2 belong to CDKB2. *CDKB1* expression is associated with S, G_2, and M phases while *CDKB2* expression is associated with G_2, and M phases. Overall, CDKB activity is widely regarded to occur during G_2/M progression. The action of CYC/CDK complexes can be regulated by CYC/CDK inhibitors (CKIs)[36,37]. There are two main families of CKIs, namely the INTERACTOR/INHIBITOR OF CDK/KIP-RELATED PROTEINs (ICK/KRPs) and the SIAMESE-RELATED PROTEINs (SMRs). ICK/KRPs consist of seven genes, *KRP1* (*ICK1*), *KRP2* (*ICK2*), *KRP3* (*ICK6*), *KRP4* (*ICK7*), *KRP5* (*ICK3*), *KRP6* (*ICK4*), *KRP7* (*ICK5*), which are distantly related to CKI p27[Kip1] protein, a member of the mammalian Kip/Cip CKI family[38]. KRPs function in a dose-dependent manner whose activity is associated with G1/S CDK inhibition primarily by inhibiting CDKA;1[37]. Meanwhile, SMRs consist of seventeen genes whose founding member, SIAMESE (SIM), was initially identified through the *sim* mutant phenotype characterized by aberrant trichome formation

wherein trichomes underwent cell division instead of endoreduplication[37,39]. KRPs have been shown to inhibit entry into both M and S phases while SMRs inhibit only the M phase[37]. How cell cycle progression affects *KNU* transcriptional activation in the context of specific cell cycle regulators have yet to be described.

It was previously shown that *del*, a 231-bp region in the *KNU* coding sequence, also plays a role in proper *KNU* temporal activation. *del* is an H3K27me3-dense region bound directly by FIE, and causes early and ectopic *KNU* expression when truncated from the *KNU* coding sequence[13]. This result suggests that the *del* region is required for *KNU* repression through H3K27me3 deposition. In this study, it is hypothesized that extension of the *KNU* coding sequence by iterative addition of the *del* region could also be sufficient for repressing *KNU* expression in a cell cycle-dependent manner, as well as in increasing the duration of temporal delay in *KNU* activation. Such manipulation would help in understanding and predicting the temporal control of gene expression during flower development, and in providing histone modification-based tools to change gene expression for developmental purposes in plants. However, such attempts have not been made yet. Here, *KNU* is demonstrated as a member of a biotimer gene regulatory network integrating AG transcriptional cascade and repressive H3K27me3 status. Novel candidate biotimer genes which belong in this regulatory network are also introduced. Finally, the critical mechanistic determinants of the biotimer, particularly the interplay of PRC2 activity, chromatin environment, and the cell cycle, are investigated by chromatin manipulation of the *KNU* coding sequence with *del*.
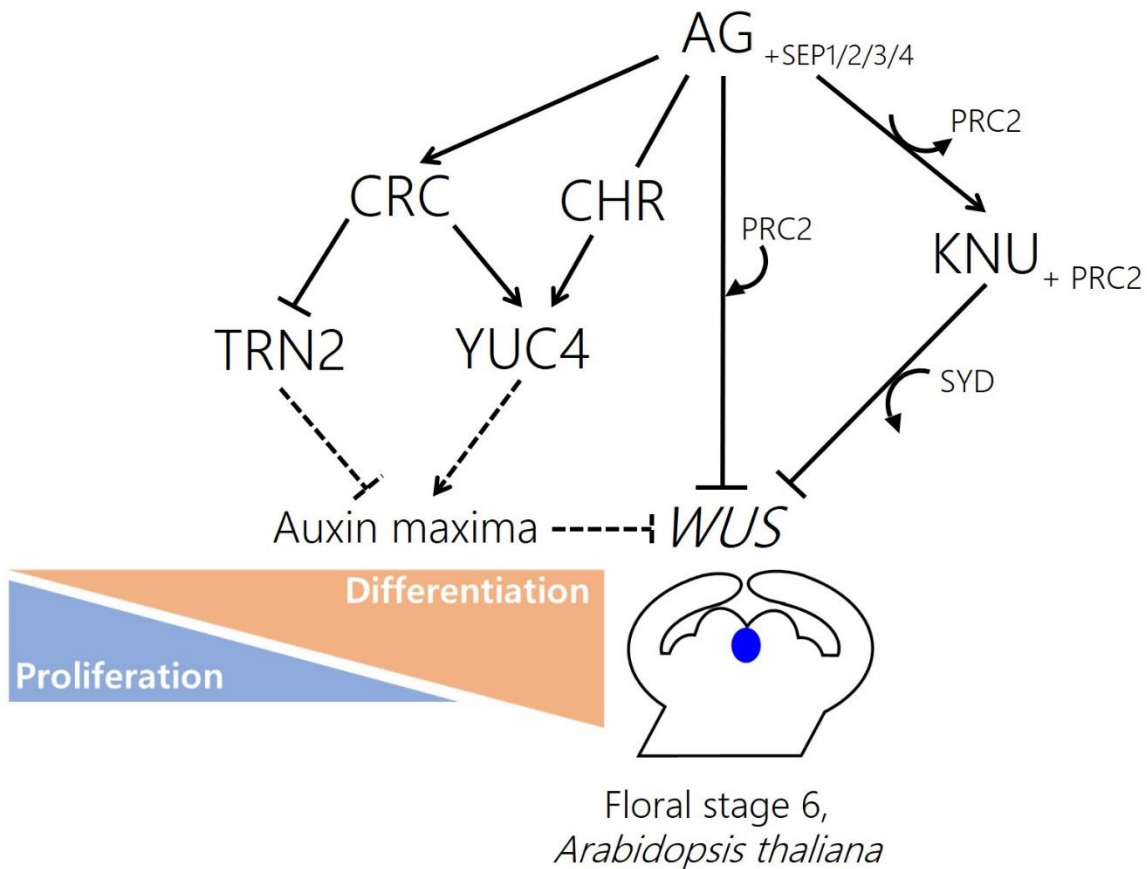
Fig. 1: Current model of gene networks regulating FM termination.

AG can directly and indirectly repress *WUS*. AG mediates PRC2 recruitment on *WUS* which directly represses *WUS*. AG indirect pathways for FM termination involves *KNU* and *CRC*. *KNU* is epigenetically activated by AG leading to PRC2 displacement from the *KNU* promoter region and subsequent H3K27me3 removal from the *KNU* coding region in a cell cycle-dependent manner. KNU (as a complex with PRC2) then directly binds on *WUS* to displace the *WUS* activator SYD and to deposit repressive H3K27me3 along the *WUS* locus. Meanwhile, AG activation of *CRC* at floral stage 6 was shown to regulate auxin homeostasis through its targets TRN2 and YUC4 (via chromatin remodeling factors (CHR)) suggesting proper auxin maxima for the transition

from cell proliferation to differentiation upon gynoecium formation is generated this way. KNU and CRC were demonstrated to synergistically regulate *WUS* repression. Solid lines indicate interactions supported by literature and dashed lines indicate interactions that are currently speculated.
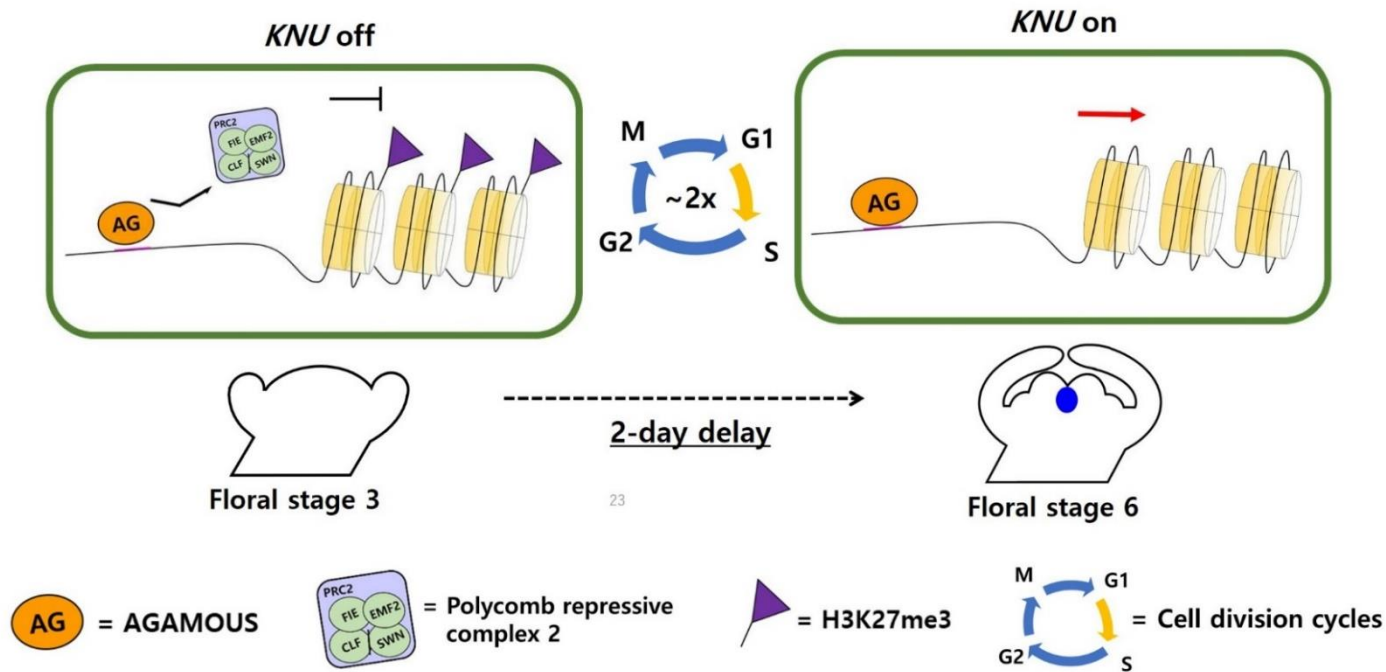
Fig. 2: Proposed biotimer model and components based on *KNU* transcriptional activation.

AG competitively binds on the *KNU* promoter region at floral stage 3 resulting in PRC2 eviction and the absence of methyl transferase activity. However, *KNU* is only fully activated at floral stage 6 when H3K27me3 marks are removed from the *KNU* coding region in a cell division-dependent manner after a 2-day delay. The proposed biotimer model is defined by its mechanistic components (represented by the legends), namely genes that are direct AG and PRC2 targets, are enriched for the H3K27me3 mark and which show transcriptional delay upon AG binding that can be associated with cell division cycles.

Materials and Methods

Plant material and growth conditions

pKNU::KNU-GUS and the *del* series, as well as the *CFP* and *2x CFP* controls, are in *A. thaliana* L*er* background. The PRC2 and cell cycle mutants used for crossing with *pKNU::KNU-GUS* and *6del* are in *A. thaliana* Col-0. *clf-28*, *cdkb1;1, cdkb1;2* are SALK T-DNA mutant lines (SALK_139371, SALK_073457 and SALK_133560, respectively), while *krp1 krp2 krp3 krp4 krp7* was previously generated from single SALK and GABI-kat lines (SALK_026391, SALK_130744, GABI-kat 185C07, SALK_102417, and GABI-kat 841D12, respectively). For *ag-1 35S::AG-GR* chemical treatment, a working concentration of 100uM dexamethasone aqueous solution was used with 0.015% Silwet L-77. Primers used for genotyping are in Table 1. Seeds were sown in pots containing soil-vermiculite mix (1:2) supplemented with Hyponex (1/1000) upon germination. Stratification at 4°C in the dark for 3-4 days was performed followed by transfer to long day conditions at 22°C and at 18°C for the lower temperature condition set up.

Table 1: Genotyping primers

Primer name	Sequence (5'-3')
Genotyping	
clf-28 F	TTCGGTTGGCACTAAACTCAC
clf-28 R	TGTAGAAGATGGACCTGCCAG
krp1 F	TCGTCGTCTTGTAGTGGAAGC
krp1 R	TGCATTTGATGTTTTTGGTTG
krp2 F	CAGTGTCGACAATGGCGGCGGTTAGGAGA
krp2 R	CAGTGCGGCCGCTCATGGATTCAATTTAACC
krp3 F	CAGTGTCGACAATGGGGGAAATACATGAAGA

krp3 R	CAGTGCGGCCGCTCATGGTTTGACTTGCAC
krp4 F	CAGTGTCGACAATGGGGAAATACATAAGAAA
krp4 R	CAGTGCGGCCGCCTAATCATCTACCTTCGTC
krp7 F	CAGTGAGCTCCAAGAGAGATTCTGAGTAC
krp7 R	CAGTGGATCCATGGCTTCTAAGGTTTC
cdkb1;1 F	CTGGTGTTGACATGTGGTCTG
cdkb1;1 R	TGTTGTAAACCATTTGTGGGC
cdkb1;2 F	AGCTTGCCTCCTAATCATCTC
cdkb1;2 R	TCAGGGCCGGCTTTACATCAAAG
SALK_LBb1.3	ATTTTGCCGATTTCGGAAC
SALK_LBb 1	GCGTGGACCGCTTGCTGCAACT
GABI-KAT_LB	ATATTGACCATCATACTCATTGC

In silico **analysis**

Transcriptomic data from Ó'Maoiléidigh et al. (2013) was filtered by setting the *p* value at < 0.05 and selecting the resulting genes from stages 3-4 and stages 6-7. Corresponding AG binding data was sorted by setting the *q*-value at < 1.0×10^{-4}. The PRC2 targets dataset[23] was filtered by selecting for the presence of CLF, EMF2, and FIE binding (features 1,2, and 3, respectively). Each of the filtered datasets was then uploaded onto a web-based custom venn diagram drawing tool (http://bioinformatics.psb.ugent.be/webtools/Venn/) to create the venn diagram. The heatmap for comparing the gene expression levels at stages 6-7 relative to stages 3-4 was generated using WebMeV (http://mev.tm4.org). The browser view of ChIP-seq signals for AG and PRC2 binding, and H3K27me3 was generated using IGV[40]. GO term analysis and visualization was performed using agriGO v2.0 (http://systemsbiology.cau.edu.cn/agriGOv2/) followed by GO term refinement using REVIGO (http://revigo.irb.hr/).

Plasmid construction and plant transformation

To create the *KNU* reporter with tandem repeats, site-directed mutagenesis was performed to insert BglII and BamHI restriction sites (+594, +1 as TSS) before the *GUS* reporter gene to create *pKNU::KNU-GUS* (BglII/BamHI). The *KNU* tandem repeat encodes partial *KNU* sequence from +367 to +594 (*1del*) and the 2X- and 3X-repeats were synthesized by GenScript Services (www.genscript.com). The synthesized 2X- and 3X-tandem repeats were digested with *Bgl*II and *Bam*HI. The *pKNU::KNU-GUS* (BglII/BamHI) construct was digested in a similar fashion. Subsequently, ligation was performed to create various constructs possessing different numbers of tandem repeats. *2del*, *3del*, *4del*, *5del* and *6del* represent the insertion of 2X-, 3X-, 4X-, 5X- and 6X-repeats, respectively. These constructs were recombined into Gateway vectors (Thermo Fisher Scientific) by LR recombination according to the manufacturer's instructions (ATMI). Primers used for cloning are listed in Table 2.

To create *gKNU-CFP-GUS* and *gKNU-2xCFP-GUS* constructs, 1XECFP and 2XECFP were amplified from pMD20-2XECFP. The resulting PCR fragments were then inserted into pCR8-pKNU::KNU-GUS (Sun et al., 2009) via a 2-step omega-PCR strategy as described by Chen, et al[41] to create pCR8-pKNU::KNU-1XECFP-GUS and pCR8-pKNU::KNU-2XECFP-GUS. Next, the vectors were introduced into CD3-694 destination vector (or pEarleyGate303) via LR reaction (Thermo Fisher Scientific).

To create *pSTY1::GUS* in the WT and in *ag-1* backgrounds, the *pSTY1* fragment was amplified from the WT *Ler* background by GXL polymerase

(Takara). The resulting promoter fragments were ligated into pENTR-dTOPO followed by heat shock transformation. Then, *pSTY1* was Gateway cloned into pPGWSF7.0 via LR reaction.

All resulting constructs were transformed into *A. thaliana Ler* via the floral dip method as described previously[42].

Table 2: Cloning primers

Primer name	Sequence (5'-3')
Cloning	
del F	GCGAGATCTACGTTTCTTCGTCCTTACCCTTG
del R	GCGGGATCCTAAACGGAGAGAAAGGTCTAGATCG
KNU-2XCFP F	CCACCCATCCTCGACGACAACAACACTAGTCATATGGATGATATCGGA
KNU-2XCFP R	GCAAGGGTAAGGACGAAGAAACGTCGACGGCCAGTGAATTCGAGCTCG
KNU-CFP F	TCTCCACCCATCCTCGACGACAACATGGTGAGCAAGGGCGAGGAGCTG
KNU-CFP R	GCAAGGGTAAGGACGAAGAAACGTCTTGTACAGCTCGTCCATGCCGAG
pSTY1 F	CACCAAGACAACAACCACCACCCATAACC
pSTY1 R	TGATCTTGGGTTGGGAAAGAATTGTGTACCGGCCATG

GUS staining

For GUS staining, the primary floral bud cluster from the main inflorescence shoot of plants approximately 3-10 cm in height were collected and fixed in ice cold 90% acetone for 20 minutes. This was followed by 2-3 times rinsing with Milli-Q H$_2$O then with a 2-3 times wash with GUS buffer (without 5-Bromo-4-chloro-3-indolyl-β-D-glucuronide/X-Gluc). The tissues were then infiltrated with GUS staining solution (with X-Gluc) under vacuum for 30 sec to 1 min minutes and incubated at 37°C for 16 hours. After incubation, the staining solution was replaced with 70% ethanol for 2-3 times until the tissues cleared (approximately 1 week).

MUG assay

To quantitatively measure GUS activity, fluorescence measurements were taken of 4-methylumbelliferyl ß-D-glucuronide (4-MUG) upon conversion to 4-methyl umbelliferone (4-MU) during GUS hydrolysis. Up to ten primary inflorescences containing floral buds until stage 12 were collected per biological replicate and flash frozen in liquid nitrogen. The procedure described by Weigel et al.[42] was followed with minor modifications. For protein extraction, the tissues were crushed upon addition of GUS extraction buffer on ice. After centrifugation, the supernatant extract was kept at -80°C until use. The remaining extract was set aside for measuring protein concentration with Qubit 4 (Thermo Fisher Scientific). For the MUG assay, the extract was added to extraction buffer mixed with 1 mM 4-MUG herein referred to as the reaction mix. Half of the reaction mix was immediately added to 0.2 M Na_2CO_3 stop buffer and designated as the 0 hr reaction. The remaining reaction mix was incubated at 37°C for 1 hr. After incubation, the reaction mix was added to the stop buffer and designated as the 1 hr reaction. The 0 hr and 1 hr reaction mix were dispensed in triplicate in 96-well plates and fluorescence measurements were taken with a TriStar[2] LB942 microplate reader (Berthold Technologies). Excitation and emission settings were at 355nm and 460nm, respectively. A 4-MU dilution series was prepared to create a 4-MU fluorescence standard curve. The samples' fluorescence signals were plotted against the standard curve and GUS protein activity was measured as the amount of substrate converted to 4-MU relative to the starting protein concentration, reaction volume, and reaction duration.

Sectioning

Following GUS staining, plant tissues were dehydrated with ethanol mixtures of increasing concentration (80%, 90%, 95%, and 100%). Embedding in Technovit 7100 resin (Heraeus) was done ATMI and 10 μm tissue sections were cut using an RM2255 microtome (Leica). The sections were dried on a 42°C hot plate (Sakura Finetek) then stained with 0.05% neutral red and mounted on a microscope slide with 500 ul MountQuick (Daido Sangyo). An Axio Scope A1 microscope (ZEISS) was used to observe the sections of three or more floral buds per flower development stage.

qRT-PCR

Total RNA was extracted from the primary floral bud cluster of the main inflorescence shoot (up to ten per biological replicate) which were harvested and ground in liquid nitrogen. RNA extraction and clean-up was performed using the RNeasy kit (Qiagen) with an in-column DNAse digest ATMI. PrimeScript RT Master Mix system (Takara) was used for cDNA synthesis and the subsequent qRT-PCR reaction mix was prepared using the FastStart Essential DNA Green Master (Roche). qRT-PCR was performed with a Light Cycler 480 (Roche) using the Light Cycler 480 release 1.5.1.62 SP software (Roche). The relative transcript abundance across three biological replicates was calculated using the comparative CT method and statistical analyses were performed using a two-tailed Student's *t*-test. Primer pair sequences for genes of interest and the reference gene *TUBULIN2* are listed in Table 3.

Table 3: qRT-PCR primers

Primer name	Sequence (5'-3')
qRT-PCR	
GUS qRT F	AGACTGTAACCACGCGTCTG
GUS qRT R	TTGTCCAGTTGCAACCACCTG
TUB2 qRT F	AAGAACCATGCACTCATCAGC
TUB2 qRT R	ATCCGTGAAGAGTACCCAGAT
KNU qRT F	ACACATCTCAAGCTCTCGGC
KNU qRT R	GTGGAGAGTTAGCGAGGACG
STY1 qRT F	CATACCTTCTCATTCAGGGCTAGA
STY1 qRT R	CTTTGAAAATGTGACCACCAATGCT
IDD12 qRT F	CCTTGCTCTTCACGTCATCA
IDD12 qRT R	CTGAGAGAGGTGGCCTTTTG
PZ10 qRT F	ATTGTTGTCTTACCATCTGTCCTCA
PZ10 qRT R	CTGTTCGTTGTGTATGGCTGAATTA
HD qRT F	GCAACGACGGAGTAATTGGT
HD qRT R	GGAGATGGCTCTTGACGTGT
AHL18 qRT F	TCCAAGAACAAACCCAAAGC
AHL18 qRT R	GAATCTCAAACCGTCCGTGT
HSP20 qRT F	TCCACTTTTCTATCTGTTGAAACATCTC
HSP20 qRT R	TAACTATAACAGGCACTGCAACGTA
KRP1 qRT F	GATCGGAAAAATCAAGCTCTGTCTC
KRP1 qRT R	TCACCATCTTTATCTTCCTCCTCCA
KRP2 qRT F	GGAAGAGAAATCGAAACGGAGAATC
KRP2 qRT R	CCATGTTCATCGATTCCTCACTCTTAT
SMR1 qRT F	AAGAGGAAGCTTTTAGTGTCGACTT
SMR1 qRT R	CTCATTGTAGACGGAGGAGAAGAAA
SMR2 qRT F	GGAGCCAAGAGGTAGAGACTTTATT
SMR2 qRT R	TGATTCAGGCACTATTACTCCTTCG
SMR3 qRT F	AGATCGAGATGTTCTTCGAGGATTT
SMR3 qRT R	CAAAGGATCAAATTACCACCACACA

ChIP

To quantify H3K27me3 and H3 enrichment, the ChIP protocol described by Yamaguchi et al.[43] was followed with minor modifications. 300-600 mg of primary inflorescences were fixed with 1% formaldehyde for 15 mins then flash

frozen with liquid nitrogen and kept at -80°C until use. Chromatin extracted by nuclei isolation was sonicated to yield 500bp fragments. Protein A beads (Thermo Fisher Scientific) were used for pre-clearing with incubation for 1 hr at 4°C on a rotating device. The beads were separated from the solution using a magnetic stand and 2/100ths was taken from the cleared solution as 2% input sample. The antibody of interest was added to the rest of the cleared solution and incubated overnight at 4°C. For immunoprecipitation, beads were added to the samples and incubated at 4°C for 6 hrs followed by washing 2x each with low salt buffer, high salt buffer, LiCl buffer, and TE buffer. Samples were incubated at 65°C for 1 hr to elute the DNA. Both the ChIP and input samples were incubated overnight at 65°C for reverse crosslinking. DNA was purified with a QIAquick PCR purification kit (Qiagen). For quantitative PCR, primers spanning the del-GUS junction yielding a 500bp amplicon was used. *EIF4* and *TA3* served as the negative control. The percent input method was used to normalize the resulting qPCR data. Primers used for qPCR are in Table 4.

Table 4: ChIP primers

Primer name	Sequence (5'-3')
ChIP	
KNU ChIP F	ACAACAACGACGGAGGAAAC
KNU ChIP R	CCAACCCGTGAAATCAAAAAA
EIF4 ChIP F	ACCAGGCGTAAGGTTGATTG
EIF4 ChIP R	GGTCCATGTCTCCGTGAGTT

Results

Genome-wide annotation of biotimer-regulated genes

"Biotimer-regulated genes" are defined to be repressed by PRC2-mediated H3K27me3 deposition prior to AG recruitment. Subsequently, H3K27me3 removal at "biotimer-regulated genes" occurs in a cell cycle-dependent manner. Thus, the biotimer model proposed in this study is defined by genes that are direct AG and PRC2 targets, are enriched for H3K27me3, and which show transcriptional delay upon AG binding associated with cell division cycles. To identify the biotimer-regulated genes which show significant transcriptional change only at stages 6-7 and are associated directly by AG, PRC2, and H3K27me3, *in silico* analysis was conducted using publicly available genome-wide datasets[18,23,44,45] (Table 5). By combining transcriptome data for an inducible *AG* loss-of-function line with a set of AG, PRC2 and H3K27me3 ChIP-seq data[18,23], 11 genes were initially found in the screen (Fig. 3). The 11 genes are enriched with AG, PRC2 and H3K27me3 and are differentially expressed in the *ag* mutant background only at stages 6-7. Since the sporogenesis gene *SPOROCYTLESS/NOZZLE* (*SPL/NZZ*) is an immediate AG target unlike *KNU*, *SPL/NZZ* was manually excluded from the final list[44,45] (Fig. 4). In this case, *SPL/NZZ* was previously shown to be induced upon 4 hours of *AG* activation[44]. Hence, 10 putative biotimer-regulated genes were annotated through *in silico* analysis (Table 6).

To gain more insight into biotimer functions, GO term analysis was carried out using the 10 putative biotimer-regulated genes[54]. Top ten GO terms generated for the 10 genes all fall under the ontology category 'Cellular Process'

and suggests the genes are mainly associated with transcription, RNA biosynthesis and metabolism, and various cellular biosynthetic processes (Fig. 5). Accordingly, subsequent GO term refinement indicates regulatory roles in transcription and development[55] (Fig. 6).

To understand stage-specific expression changes of these 10 genes, k-means clustering was performed. Gene expression analysis at stages 6-7 (relative to stages 3-4) sorts these genes into two different clusters based on upregulation or downregulation (Fig. 7). The upregulated cluster contains two genes that encode *SHOOTMERISTEMLESS* (*STM*) and *ZINC FINGER PROTEIN 1* (*ZP1*)[46,47]. The remaining eight genes are in the downregulated cluster. This result suggests that majority of these genes remain transcriptionally repressed without a functional AG and that repression may be accounted for by non-removal of H3K27me3 marks. With the exception of *AT4G16540* and *AT3G11150* (a heat-shock protein and oxygenase protein, respectively), six genes in the downregulated cluster are either characterized transcription factors or associated with DNA-binding transcription factor activity[48–50]. Three of the genes encode zinc finger proteins, namely *KNUCKLES* (*KNU*), *INDETERMINATE DOMAIN 12* (*IDD12*), and *STYLISH 1* (*STY1*)[12,19,51]. The remaining three genes are *PLATZ10*, *AT1G14600*, and *AT-HOOK MOTIF NUCLEAR-LOCALIZED PROTEIN 18* (*AHL18*), which encode a PLATZ transcription factor, a homeodomain-like protein, and an AT hook domain containing protein, respectively[21,51–53].

To understand the mechanistic determinants of the biotimer, specifically how AG, PRC2, and H3K27me3 interactions affect the chromatin landscape and the resulting control of transcriptional activation, AG, PRC2, and

H3K27me3 binding patterns was visualized along the loci of selected candidate genes (Fig. 8). This set comprises well-characterized genes from the list which are all implicated in various stages of flower development (*AHL18*, *IDD12*, and *STY1*) along with *KNU* as a control. As reported previously, AG directly binds to the 5' region of the *KNU* promoter. PRC2 binding and H3K27me3 at *KNU* were observed in the gene body (Fig. 8a). These confirm previous findings about *KNU* transcriptional regulation and leads us to the questions 1) How much of what is known from *KNU*'s biotimer regulation applies to the other candidate genes? and 2) What other factors could be contributing to the biotimer mechanism? It was observed that AG significantly binds upstream of the genes *AHL18*, *IDD12*, and *STY1* (Fig. 8b-d). Likewise, significant PRC2 binding and H3K27me3 signals were detected in the gene body of these three genes (Fig. 8b-d).

Initial *in planta* analysis was performed with selected candidate genes via time-course gene expression analysis with the inducible *AG* line *ag-1 35S::AG-GR* (Fig. 9). The expression levels for *IDD12*, *AHL18, PZ10*, *STY1*, *HD*, and *HSP20* (with *KNU* as a control) were quantified over a seven-day period from 0 hour (0h) of no dexamethasome (dex) treatment (NT) then at 1 day after treatment (1d T), and alternately at 3 days (3d T), 5 days (5d T) and at 7 days (7d T). *KNU*'s expression profile is significantly upregulated at 3d after dex treatment consistent with the transcriptional delay that characterizes *KNU* activation (Fig. 9a). A transcriptional delay was observed for *IDD12*, *AHL18, PZ10*, *STY1*, and *HD* (Fig. 8b-f). For *IDD12*, *AHL18*, and *PZ10*, significant increase in gene expression was observed at 3d after treatment (Fig. 9b-d).For *STY1* and *HD*, significant increase in gene expression was observed at 7d after

treatment (Fig. 9e-f). An additional set of gene expression analysis including 2 days after treatment (2d T) was made for *KNU*, *IDD12*, and *PZ10* showing that *IDD12* activation begins at 2d after treatment. Meanwhile, *KNU* and *PZ10* activation begins at 3d after treatment (Fig. 10). Results of this initial *in planta* analysis suggests that among these candidate genes, *IDD12*, *PZ10*, and *AHL18* show the most similarity to *KNU* transcriptional regulation characterized by 1-2 days of transcriptional delay upon *AG* activation.

  STY1, a well-characterized regulator of carpel development, was initially selected to observe its stage-specific expression pattern from floral stages 4-8 by introducing the promoter fusion *pSTY1::GUS* construct in the WT and *ag-1* background (Fig. 11). *STY1* expression can be observed from stage 4 at the tips of the nascent floral organs marking the apical region of the developing carpel in the succeeding stages and corresponds to previous *in situ* hybridization results (Fig. 11a-e)[19]. This suggests that the observed delay in *STY1* expression in *ag-1 35S::AG-GR* may be the result of a time lag until transcript accumulation is quantifiable at later stages rather than as a transcriptional delay resulting from biotimer regulation. However, whether the observed *STY1* tissue-specific expression pattern is a result of biotimer regulation or otherwise remains to be elucidated. A transcriptional fusion approach by cloning the entire gene and upstream regions may be an additional strategy to observe the spatiotemporal endogenous gene expression pattern, wherein possible regulatory regions excluded in the promoter fusion lines can be included. This also highlights the need to observe the stage-specific tissue expression pattern of the other candidate genes to confirm biotimer regulation.

Overall, *in silico* analysis of publicly available genome-wide data sets yielded 10 biotimer-regulated candidate genes and initial *in planta* analysis revealed further insight into biotimer regulation. These data suggest a probable biotimer mechanism during early flower development that integrates H3K27me3 status within a gene regulatory network downstream of the floral homeotic C class gene *AG*.

Table 5: Genome-wide datasets used for *in silico* analysis

| Dataset	Genotype	Tissue developmental stage	Number of genes	References
Early floral stage microarray	35S$_{PRO}$:AP1-GR *ap1-1cal-1*	Stages 3-4	245	Ó'Maoiléidigh et al, 2013
		Stages 5-6	920	Ó'Maoiléidigh et al, 2013
AG ChIP	AP1$_{PRO}$:AP1-GR AG$_{PRO}$:AG-GFP *ap1-1 cal-1 ag-1*	~Stage 5	2224	Ó'Maoiléidigh et al, 2013
PRC2 and H3K27me3 ChIP	Wild type, PRC2 mutants and tagged lines	Seedlings	1416	Xiao et al, 2017
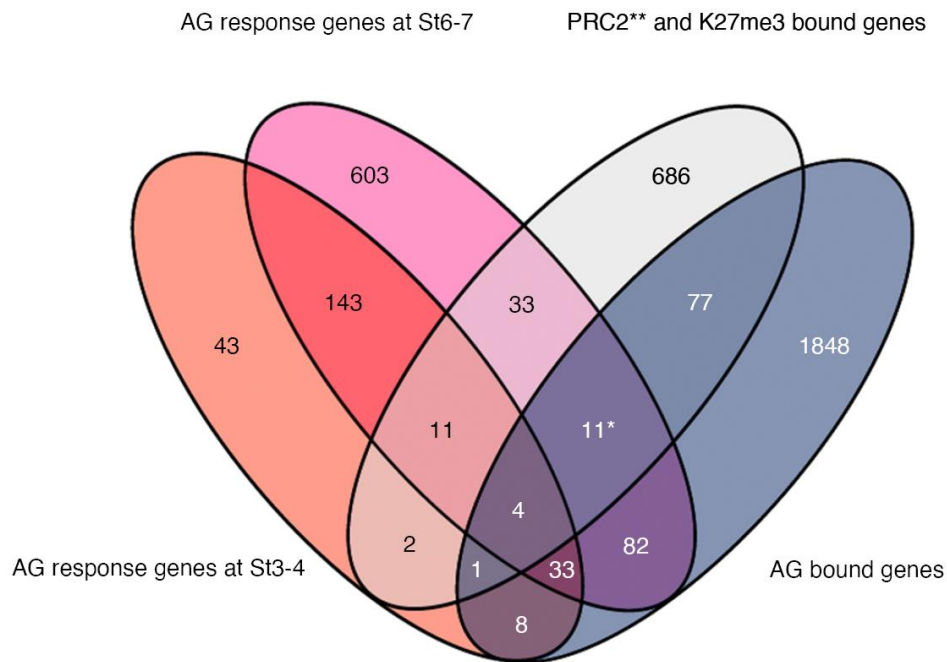
Fig. 3: Venn diagram showing the gene clusters generated when the selection criteria was applied.

The 11 identified biotimer-regulated genes are indicated by an asterisk. These are AG-response genes which show significant transcriptional change at stages 6-7, are bound directly by AG and PRC2 components, and are marked by H3K27me3.
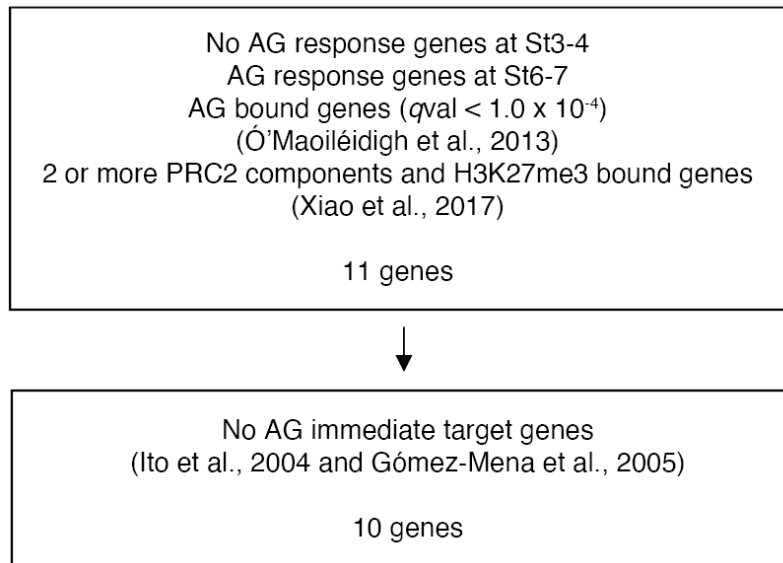
```
┌────────────────────────────────────────────────────┐
│           No AG response genes at St3-4             │
│           AG response genes at St6-7                │
│        AG bound genes (qval < 1.0 x 10⁻⁴)           │
│             (Ó'Maoiléidigh et al., 2013)            │
│  2 or more PRC2 components and H3K27me3 bound genes  │
│                 (Xiao et al., 2017)                 │
│                                                      │
│                     11 genes                        │
└────────────────────────────────────────────────────┘
                          ↓
┌────────────────────────────────────────────────────┐
│           No AG immediate target genes              │
│   (Ito et al., 2004 and Gómez-Mena et al., 2005)    │
│                                                      │
│                     10 genes                        │
└────────────────────────────────────────────────────┘
```

Fig. 4: Schematic representation of reference datasets used and the selected criteria for filtering biotimer-regulated genes of interest.

The following four publicly available genome-wide data sets that correspond to the biotimer definition were used to annotate candidate biotimer genes, namely flower stage specific transcriptome data from an inducible *AG* loss-of-function line (*35S$_{PRO}$:AP1-GR ap1-1cal-1*), ChIP data for AG (AP1$_{PRO}$:AP1-GR AG$_{PRO}$:AG-GFP *ap1-1 cal-1 ag-1*) and PRC2 binding, as well as H3K27me3 enrichment data (wild type, PRC2 mutants and tagged lines). The criteria used to screen these datasets were significant gene expression change in stages 6-7 (relative to stages 3-4), and significant AG & PRC2 binding, and H3K27me3 enrichment resulting in 11 candidate genes. Genes that were previously identified as immediate AG targets was added as a final criterion to screen the resulting candidate gene list for a total of 10 genes.
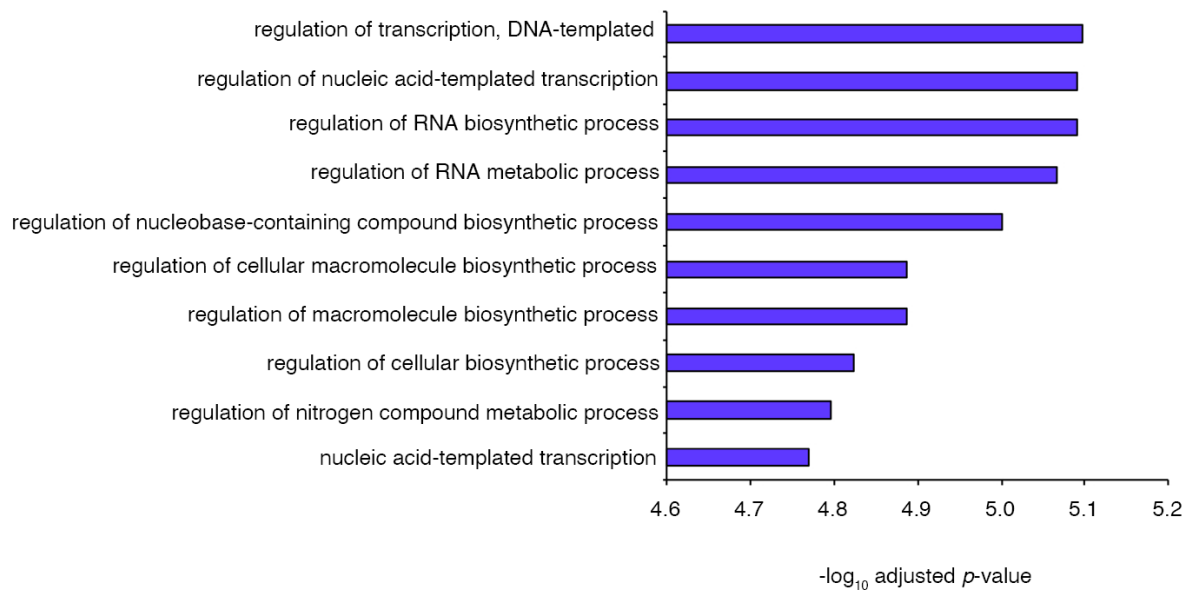
Fig. 5: Top ten GO terminology for the identified biotimer-regulated genes (excluding *SPL/NZZ*) generated using agriGO v2.0.

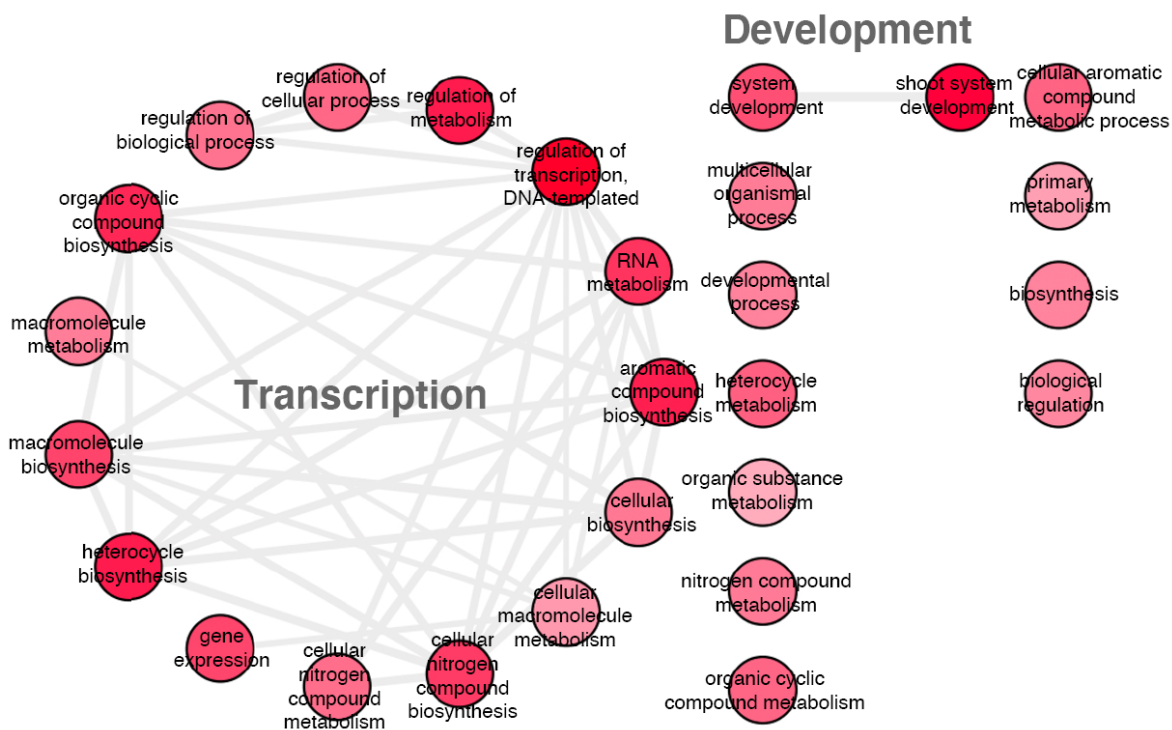The functional enrichment ranking is based on the *p*-values of significant GO terms.

Fig. 6: Graph-based visualization of refined GO terminology using REViGO.

The node radius indicates specificity and the color shading corresponds to the *p*-values provided in REViGO (higher red intensity indicates smaller *p*-values). Highly similar GO terms are linked by edges where edge thickness signifies the degree of similarity.
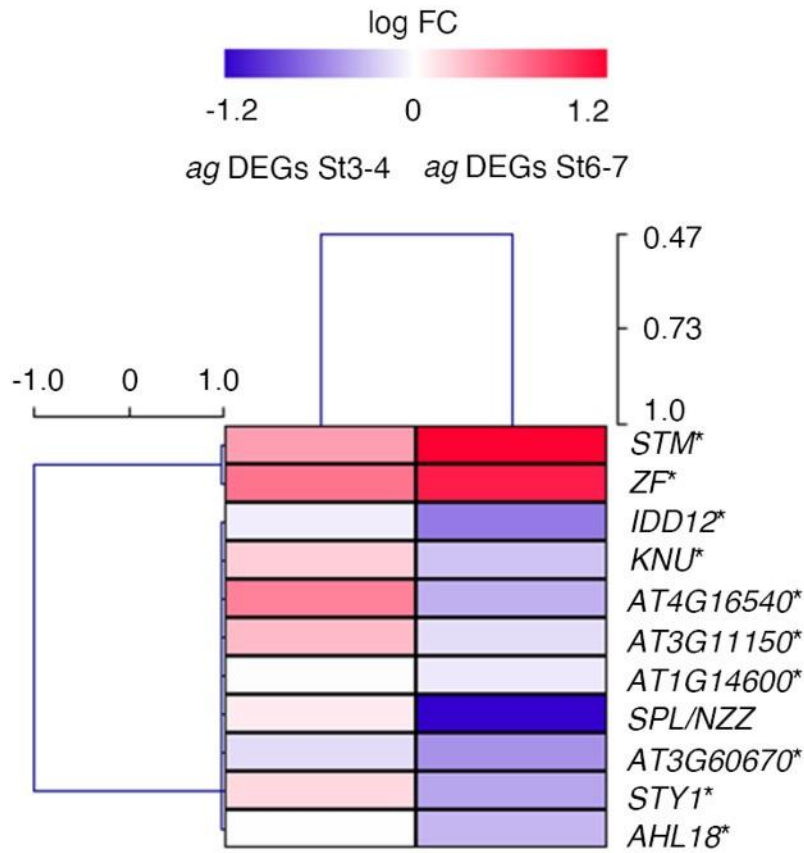
Fig. 7: Transcriptional heatmap of the 11 identified biotimer-regulated genes.

Significant transcriptional change occurs for all genes at stages 6-7 relative to stages 3-4 (vertical clustering, log fold change (FC) from -1.2 to 0.29). Two genes are upregulated by stages 6-7 (*STM* and *ZF*) while the rest show downregulation (horizontal clustering, log FC from -1.0 to 1.0).
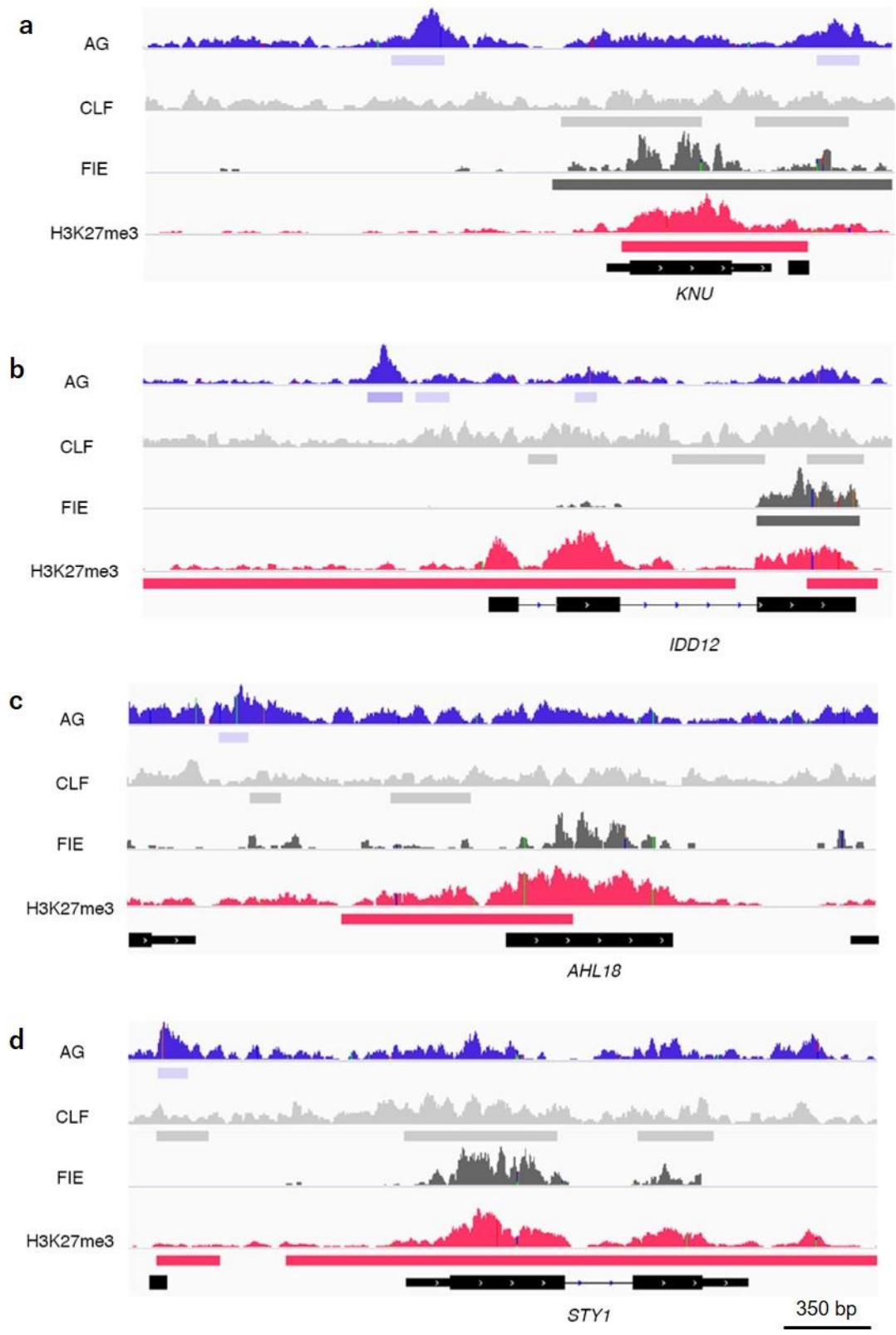
KNU

IDD12

AHL18

STY1

350 bp

Fig. 8: Input-subtracted ChIP-seq signals for AG, PRC2 components CLF and FIE, and H3K27me3.

Binding patterns for AG, PRC2 and H3K27me3 were visualized for *KNU* (**a**), *IDD12* (**b**) *AHL18* (**c**), and *STY1* (**d**) using Integrative Genomics Viewer (IGV). Solid horizontal bars below the peaks indicate regions with significant binding along the loci. The gene coding regions are indicated by the black bars transected by light blue arrows at the bottom of each panel (the transected lines between the bars represent introns). Scale bar = 350 base pairs (bp)

Table 6: Candidate biotimer genes

| AGI code	Gene name	Biochemical function and/or protein type	References
AT1G62360	*SHOOTMERISTEMLESS* (*STM*)	Shoot apical meristem maintenance, floral meristem specification	[34]
AT4G02670	*INDETERMINATE DOMAIN 12* (*IDD12*)	Transcription factor	[39]
AT4G17810	*ZINC FINGER PROTEIN 1* (*ZP1*)	Root hair development	[35]
AT5G14010	*KNUCKLES* (*KNU*)	Floral meristem termination	[10]
AT4G16540	*HEATSHOCK PROTEIN 20* (*HSP20*)	Flower development	[37, 38]
AT3G11150	N/A	Chloroplast functions (2-oxoglutarate (2OG) and Fe(II)-dependent oxygenase superfamily protein)	[36]
AT1G14600	N/A	Homeodomain transcription factor	[39, 42]
AT3G60670	*PLATZ10* (*PZ10*)	Putative transcription factor	[41]
AT3G51060	*STYLISH 1* (*STY1*)	Gynoecium development	[40]
AT3G60870	*AT-HOOK MOTIF NUCLEAR-LOCALIZED PROTEIN 18* (*AHL18*)	Flowering	[43]

N/A: not applicable
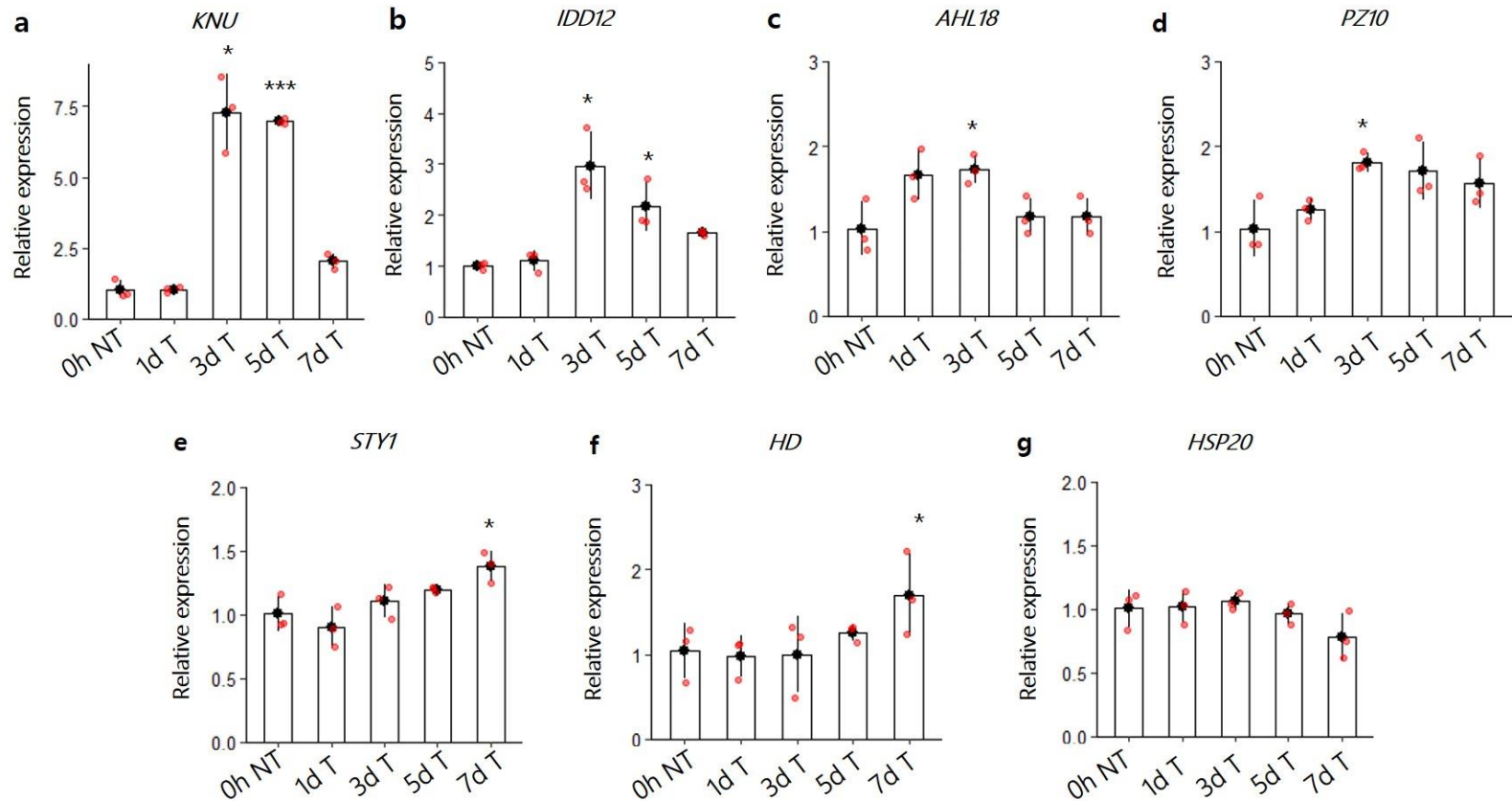
Fig. 9: Time-course gene expression analysis in the inducible *AG* line *ag-1 35S::AG-GR* for selected candidate genes determined by qRT-PCR.

Transcript accumulation was determined for *KNU* (**a**), *IDD12* (**b**), *AHL18* (**c**), *PZ10* (**d**), *STY1* (**e**), *HD* (**f**), and *HSP20* (**g**) at the following time points: 0 hour with no dexamethasone treatment (0h NT), 1 day after dexamethasone treatment (1d T), 3 days after treatment (3d T), 5 days after treatment (5d T), and 7 days after treatment (7d T). Data represent average fold changes ± standard errors of three biological replicates (n = 3). $2^{-\Delta\Delta Ct}$ method was used to calculate the fold change in gene expression for 1d T to 7d T samples relative to 0h NT. Significant differences were determined using a two-tailed Student's *t*-test (***** = $p < 0.05$, ******* = $p < 0.001$). *TUB2* served as the reference transcript.
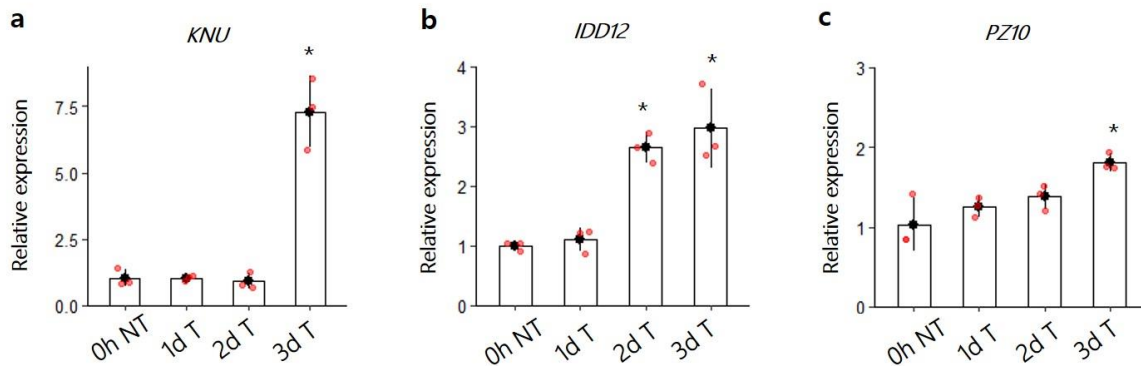
Fig. 10: Additional time-course gene expression analysis in the inducible AG line *ag-1 35S::AG-GR* for selected candidate genes determined by qRT-PCR.

2 days after dex treatment (2d T) is included in this time course analysis for *KNU* (**a**), *IDD12* (**b**)*,* and *PZ10* (**c**). The time points for checking transcript accumulation were 0 hour with no dex treatment (0h NT), 1 day after dex treatment (1d T), 2 days after dex treatment (2d T) and 3 days after dex treatment (3d T). RNA was isolated from floral bud clusters containing flowers until stage 12. Data represent average fold changes ± standard errors of three biological replicates (n = 3). $2^{-\Delta\Delta Ct}$ method was used to calculate the fold change in gene expression for 1d T to 3d T samples relative to 0h NT. Significant differences were determined using a two-tailed Student's t-test (* = p < 0.05, ***= p < 0.001). *TUB2* served as the reference transcript.
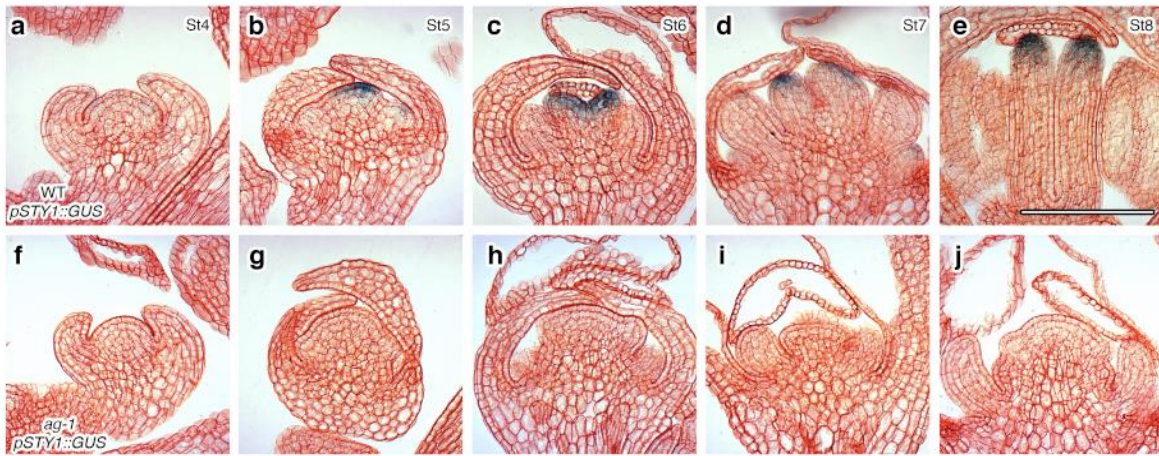
Fig. 11: Stage-specific gene expression pattern for *STY1*.

Representative longitudinal GUS sections from stage 4 to 8 of WT *pSTY1::GUS* (**a-e**) and *ag-1 pSTY1::GUS* floral buds (**f-j**). Cell walls were stained with neutral red dye. Scale bar = 50 µm.

Extending the *KNU* coding region with *del* delays and reduces *KNU* temporal activation

In this study, it was hypothesized that extension of the *KNU* coding sequence increases the repressive H3K27me3 marks and further delays the induction of *KNU* during floral development based on the previous observation that deleting a 231 bp region (*del*) leads to precocious and ectopic *KNU* expression. To examine this hypothesis, the 231 bp deletion region (*del*) was introduced into the *pKNU::KNU-GUS* construct iteratively (Fig. 12). For the generated T1 lines each containing one of the variant *del* constructs (*1del* to *6del*), the GUS signal intensity was determined from floral stage 6 to 8 and categorized into either weak, intermediate, or strong groups depending on signal strength (Fig. 13). Specifically, a weak signal intensity was defined as when no signal is observed from stage 6 floral buds. An intermediate signal intensity is when a minimal signal from stage 6 was detected and strong signal intensity is when GUS expression is clearly detected from stages 5-6 floral buds. The highest occurrence of a strong GUS signal was observed for the *pKNU::KNU-GUS* lines while the frequency of a strong GUS signal among the lines decreased as the number of *del* regions increased (Fig. 14). *1del* to *3del* show similar GUS signal frequencies, as well as for *4del* to *6del* suggesting that the effect of *del* addition has a threshold on modulating GUS signal intensities. Meanwhile, extending the *KNU* coding region with *CFP* and *2XCFP,* with comparable lengths to *3del* and *6del* respectively, led to similar T1 GUS signal intensities with *pKNU::KNU-GUS* (Fig. 15) suggesting that the temporal delay in GUS accumulation is regulated in a *del*-specific manner. Representative *pKNU::KNU-GUS, 3del,* and *6del* homozygous lines were used to characterize

spatial GUS expression during flower development (Fig. 16). In *pKNU::KNU-GUS*, *KNU* induction was observed starting at floral stage 5 showing a moderate GUS signal (Fig. 16d) then proceeded to a strong GUS signal at stage 6 (Fig. 16e). A moderate signal was observed from stage 7 to 8 (Fig. 16f-g). This expression pattern corresponds to the timing of *KNU* mRNA accumulation in WT plants[12]. For *3del*, only a weak GUS signal was observed at the center of the floral meristem at stage 5 (Fig. 16i). This weak signal continues onto stage 6 until a moderate signal is observed at stage 7 and weakly observed at stage 8 (Fig. 16j-l). *6del* also showed a weak GUS signal initially seen at stage 6 until stage 7 and attenuates by stage 8 (Fig. 16o-q). Based on quantitative reverse transcription PCR (qRT-PCR), *GUS* transcript levels were significantly decreased in *6del* compared to *pKNU::KNU-GUS* (Fig. 17), while endogenous *KNU* expression between the two were comparable and showed no significant difference (Fig. 18). Furthermore, fluorimetric detection of GUS activity levels by ß-D-Galactopyranoside (MUG) assay showed significantly decreased GUS activity in *6del* compared to *pKNU::KNU-GUS* (Fig. 19). These results demonstrate that increasing the *KNU* coding sequence with iterative addition of the *del* sequence can prolong the delay and also reduces *KNU* expression.

To gain insight into the tri-methylation status of histone H3 Lys27 between *pKNU::KNU-GUS* and *6del*, H3K27me3 chromatin immunoprecipitation (ChIP) followed by quantitative real-time PCR (qPCR) (ChIP-qPCR) was performed. The results from these experiments showed enriched H3K27me3 levels for *6del* mutants compared with *pKNU::KNU-GUS* (Fig. 20). H3 ChIP for both lines showed similar H3 enrichment (Fig. 21), suggesting that H3 levels are not changed in these two lines and the observed

difference is due to the deposition of tri-methylation marks. These results suggest that this delay in *KNU* activation is due to increased repressive H3K27me3 deposition as the *KNU* coding sequence is extended.
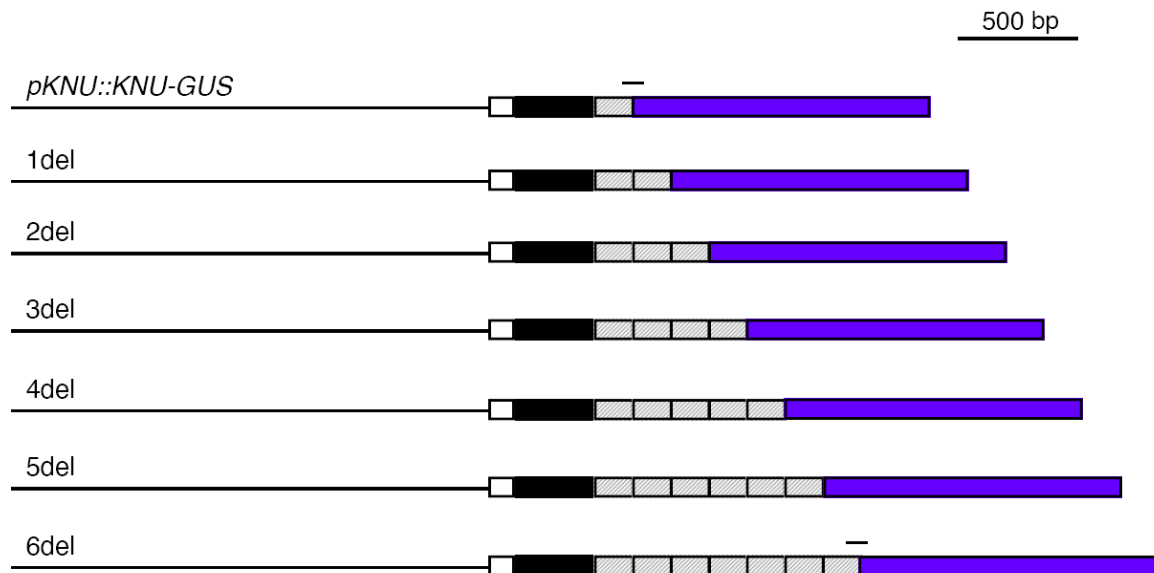
Fig. 12: Schematic construct diagrams of the *KNU-GUS* series.

The solid black line is the region upstream of the *KNU* coding sequence. The succeeding white, black, gray, and blue bars represent the 5'-UTR, 255 bp *KNU* coding sequence, 231 bp *del* sequence and *GUS* gene, respectively. The gray bars correspond to *1del* through *6del*. The scale bar above the *del* and *GUS* gene junction on *pKNU::KNU-GUS* and *6del* is a 500 bp PCR amplicon and for ChIP-qPCR.

Fig. 13: Representative variant *del* T1 lines displaying the characteristic GUS signal levels for classifying *pKNU::KNU-GUS* and *del* T1 lines

GUS signal intensity was observed from floral stage 6 to 8 and categorized into weak signal intensity (**a**) when no signal is observed from stage 6 floral buds, intermediate signal intensity (**b**) when a minimal signal from stage 6 was detected and strong signal intensity (**c**) when GUS expression is clearly detected from stages 5-6 floral buds.
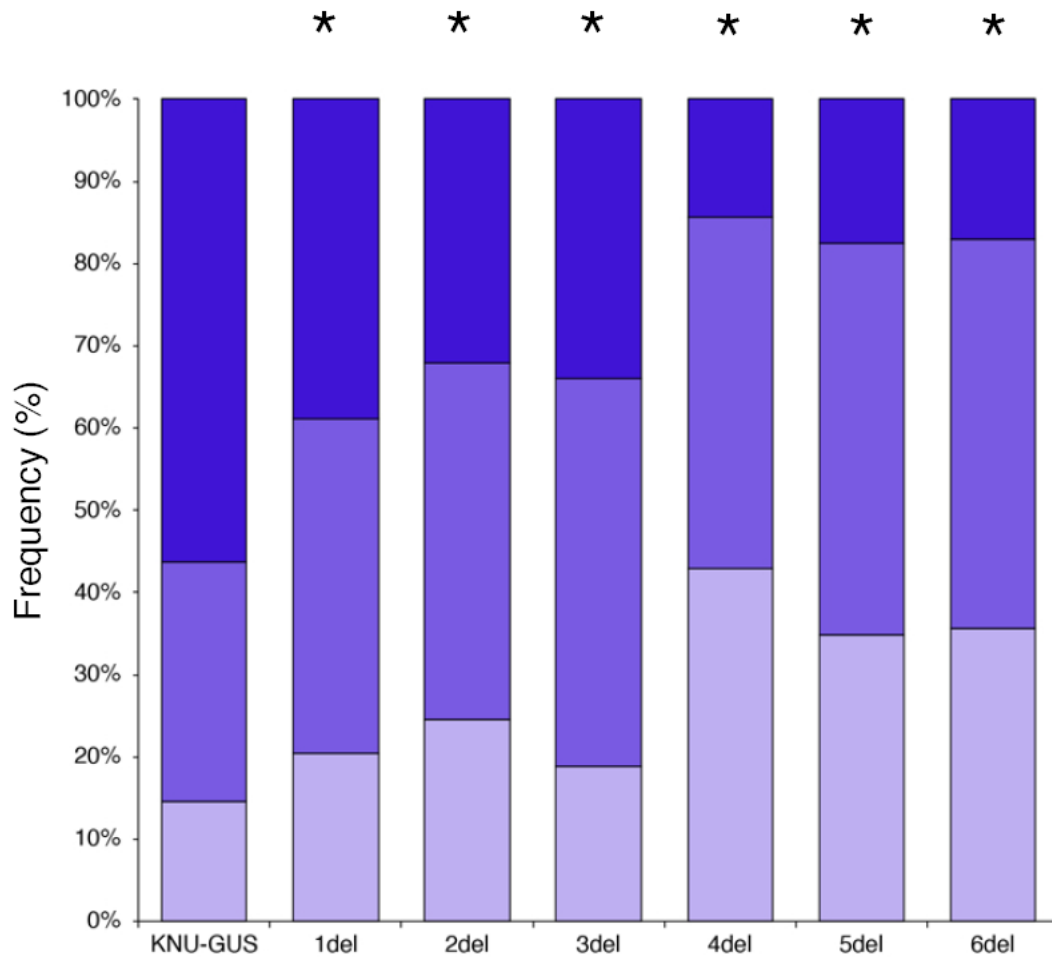
Fig. 14: Variation in GUS expression levels in *pKNU::KNU-GUS* and *del* T1 lines.

The blue, light blue, and gray bars represent strong, intermediate, and weak GUS signal intensity, respectively. X^2 test was used to show significant differences among the del lines (n > 35, *$p < 0.05$).
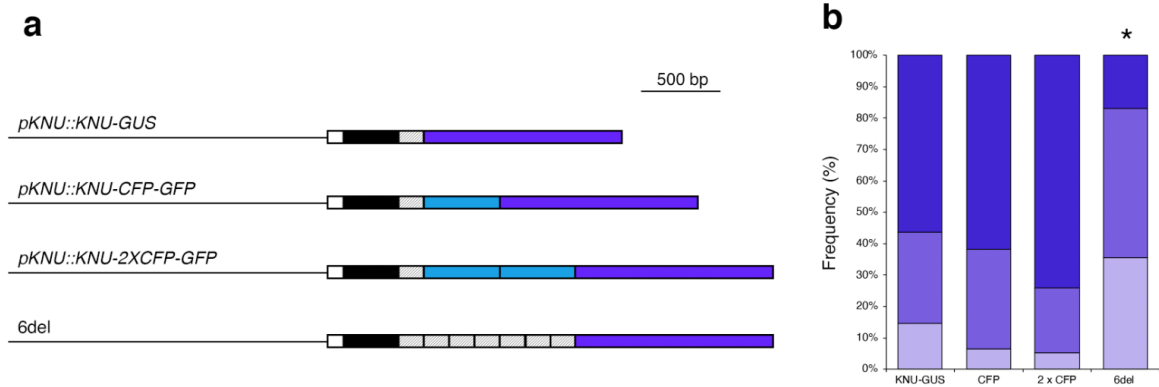
Fig. 15: *KNU* **extended with** *CFP* **and** *2XCFP* **resulted in similar T1 GUS signal intensities with** *pKNU::KNU-GUS*

(**a**) Graphical representations of the *pKNU::KNU-CFP-GFP* and *pKNU::KNU-2XCFP-GFP* constructs relative to *pKNU::KNU-GUS* and *6del*. For *pKNU::KNU-CFP-GFP* and *pKNU::KNU-2XCFP-GFP*, the solid black line is the region upstream of the *KNU* coding sequence. The succeeding white, black, gray, and light blue bars represent the 5'-UTR, 255 bp KNU coding sequence, 231 bp del sequence and *CFP* or *2XCFP* gene.

(**b**) Variation in GUS expression levels in *pKNU::KNU-CFP-GFP* and *pKNU::KNU-2XCFP-GFP* compared with *pKNU::KNU-GUS* and *6del* T1 lines. The blue, light blue, and gray bars represent strong, intermediate, and weak GUS signal intensity, respectively. X^2 test was used to show significant differences among the *del* lines (n > 35, *$p < 0.05$).
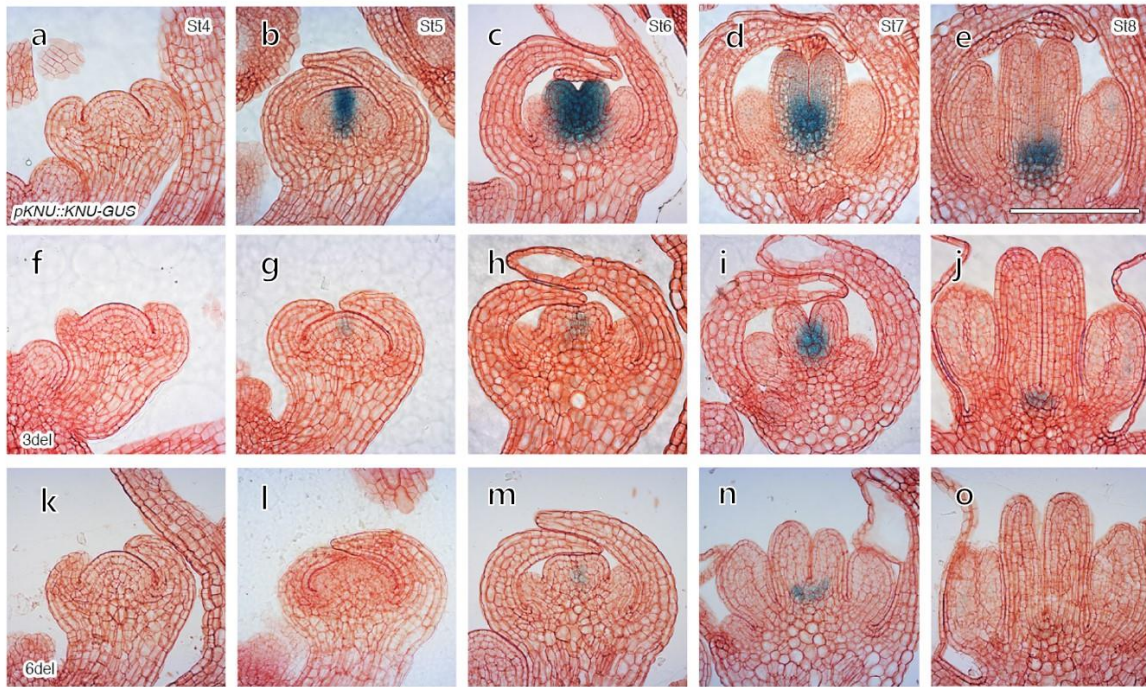
47

Fig. 16: Floral stage-specific *KNU-GUS* expression pattern in WT, *3del* and *6del*.

Representative longitudinal GUS sections from stage 4 to 8 of *pKNU::KNU-GUS* (**a-e**)*, 3del* (**f-j**)*,* and *6del* (**k-o**) floral buds. Cell walls were stained with neutral red dye. Scale bar = 50 µm.
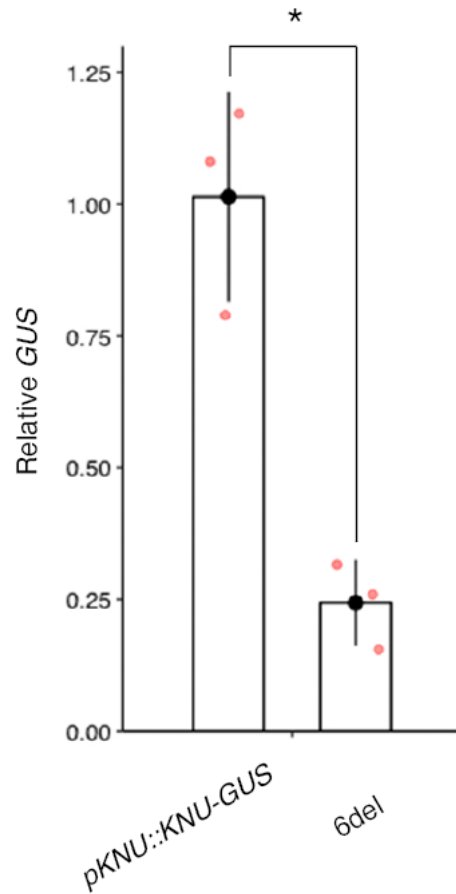
Fig. 17: *GUS* **transcript levels in** *pKNU::KNU-GUS* **and** *6del* **determined by qRT-PCR.**

Data represent average fold changes ± standard errors of three biological replicates (n = 3). Significant differences were determined using a two-tailed Student's *t*-test ($p < 0.05$). *TUB2* served as the reference transcript.
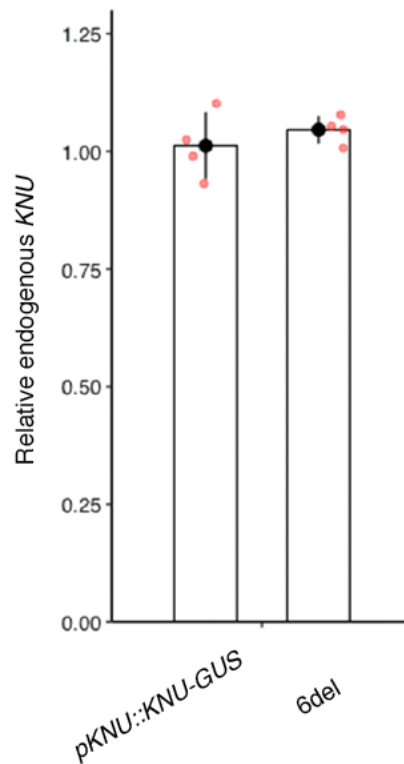
Fig. 18: Endogenous *KNU* mRNA accumulation in *pKNU::KNU-GUS* and *6del* are similar

Endogenous *KNU* transcript levels in *pKNU::KNU-GUS* and *6del* determined by quantitative reverse transcription PCR (qRT-PCR) using RNA isolated from floral bud clusters containing flowers until stage 6. Data represent average fold changes $\pm$ standard errors of three independent experiments (n = 4). *TUB2* served as the reference transcript.
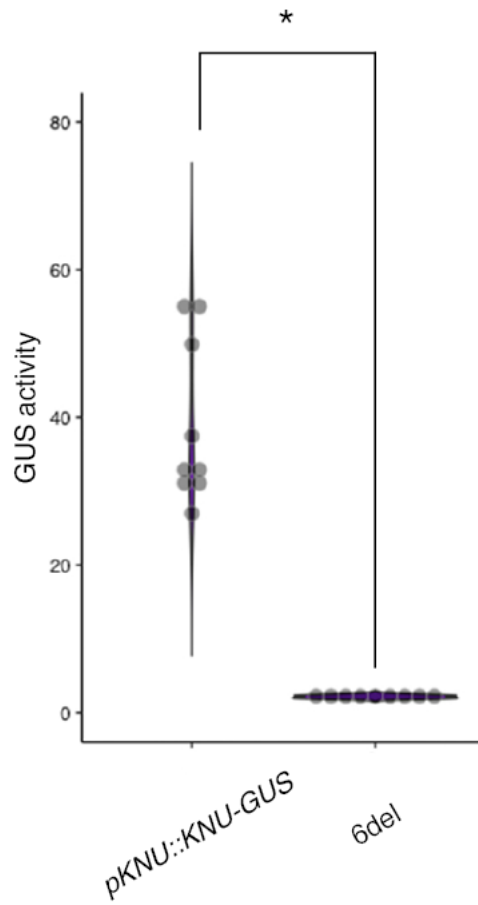
Fig. 19: GUS protein activity determined by MUG assay.

Data represent average of GUS activity (nmol/mg/h) ± standard errors from nine biological replicates (n = 9). Significant differences were determined using a two-tailed Student's t-test ($p < 0.05$).
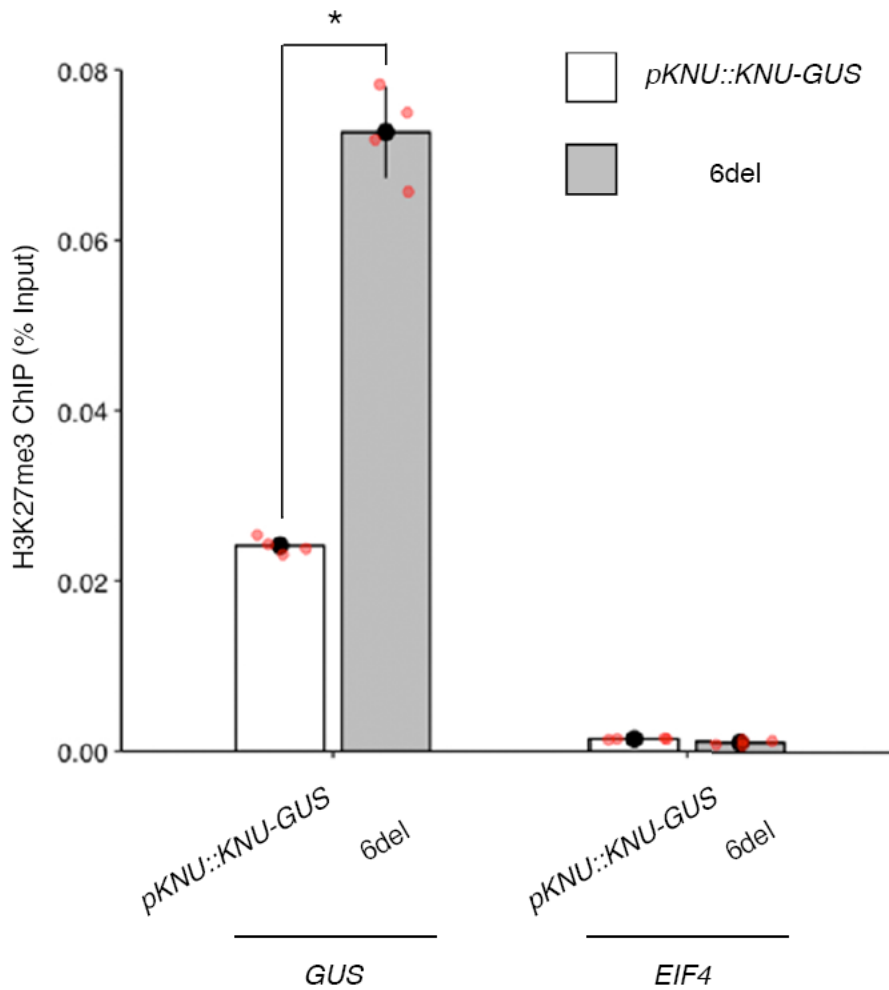
Fig. 20: H3K27me3 enrichment in *pKNU::KNU-GUS* and *6del*

Data represent average of % Input ± standard errors from four biological replicates n = 4). Significant differences were determined using a two-tailed Student's *t*-test ($p < 0.05$). *EIF4A1* served as the negative control.

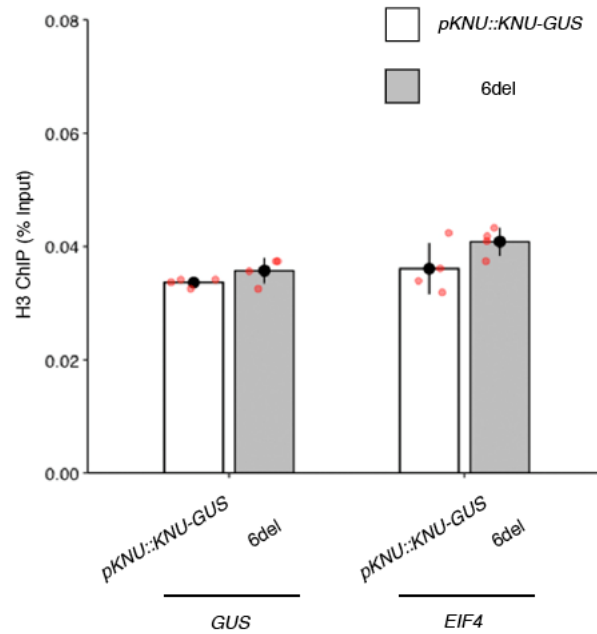**Fig. 21: Occurrence of the histone variant H3 are similar in *pKNU::KNU-GUS* and *6del*.**

H3 enrichment in *pKNU::KNU-GUS* and *6del* using floral bud clusters containing flowers until stage 10. Data represent average of % Input ± standard errors from three independent experiments (n = 4). A two-tailed Student's *t*-test was used to determine significant differences ($p < 0.05$). *EIF4A1* served as the positive control.

PRC2 deposits H3K27me3 on the extended *KNU* coding sequence

6del expression in WT was observed to initiate at stage 6 of floral development with delay (Fig. 16). In this case, *6del* displayed the most apparent change in *KNU* temporal activation compared with the other members of the *del* series (such as *3del*). Hence, to determine if PRC2 is responsible for H3K27me3 deposition on the extended *KNU* coding sequence leading to further delay in *KNU* expression, the effects on *6del* by PRC2 (FIE and CLF) activity was investigated (Fig. 22). Since loss-of-function mutants of the *FIE* gene are embryonic lethal, the co-suppression mutant *p35S::GFP-FIE* (hereinafter referred to as *fie*) with reduced *FIE* levels was used as an alternative[56]. *6del* was also crossed into the PRC2 mutant *clf-28* (*clf*) (Fig. 22k-o). In WT, the *6del* signal was not detected at stage 4 and 5 (Fig. 22a and b). Then, the *6del* signal in WT was first observed at stage 6 and was weakly maintained until stage 7 (Fig. 22c and d). There is little to no GUS signal observed at stage 8 (Fig. 22e). Although no GUS signal was detected at stage 4, *6del* was precociously expressed in *fie* and *clf* at stage 5 (Fig. 22b, g and l). The *6del* signals were maintained at higher levels at stage 6 and 7 in *fie* and *clf* compared to those in WT (Fig. 22c, d, h, i, m and n). The *6del* signal appeared to attenuate by stage 8 in WT and *clf* (Fig. 22e and o). The lower induction levels in *clf* may be accounted for by *clf-28* as a *clf* loss-of-function allele that exhibits the typical PRC2 mutant phenotypes, but to a moderate degree[57,58]. GUS accumulation was still observed at stage 8 in the *fie* background (Fig. 22j). Meanwhile, *pKNU::KNU-GUS* in the *clf-28* background showed no apparent differences in GUS expression from stages 4-8 compared to *pKNU::KNU-GUS* in the WT background (Fig. 23). Previous data showed that *AG* was ectopically induced

in vegetative leaves in the *fie* co-suppression line, as well as in the *clf/swn* double mutant line (approximately 30-fold increase)[13]. In these PRC2 mutant backgrounds, *KNU* is also ectopically induced but not as strongly as *AG* (approximately 2-fold increase)[13]. Ectopic *AG* expression also did not lead to ectopic *KNU* expression in early stage floral buds or vegetative leaves in the inducible *pKNU::KNU-GUS ag-1 35S::AG-GR* line[13]. These suggest that *KNU* activation is dependent on loss of PRC2 activity and may account for the similar *KNU* expression pattern observed between WT and *clf-28*. In *clf-28*, PRC2 activity is only moderately reduced and SWN function remains intact.

GUS transcript accumulation was then quantified for *fie* relative to *6del* WT. Consistent with the precocious and ectopic *GUS* expression observed for *fie* compared to *6del* WT, significant increase in *GUS* transcripts in *fie* was observed through qRT-PCR (Fig. 24).

To examine whether increased repressive H3K27me3 deposition on extended *del* regions depends on the PRC2 activity, H3K27me3 levels in the PRC2 mutant background was checked by ChIP-qPCR. H3K27me3 levels on *6del* in *fie* were significantly lower compared to that in WT (Fig. 25). Furthermore, H3K27me3 levels on *6del* in *clf* and *fie* were significantly lower than WT (Fig. 25). Hence, the increase in *GUS* expression is due to the disrupted PRC2 machinery leading to attenuated H3K27me3 deposition on target loci.
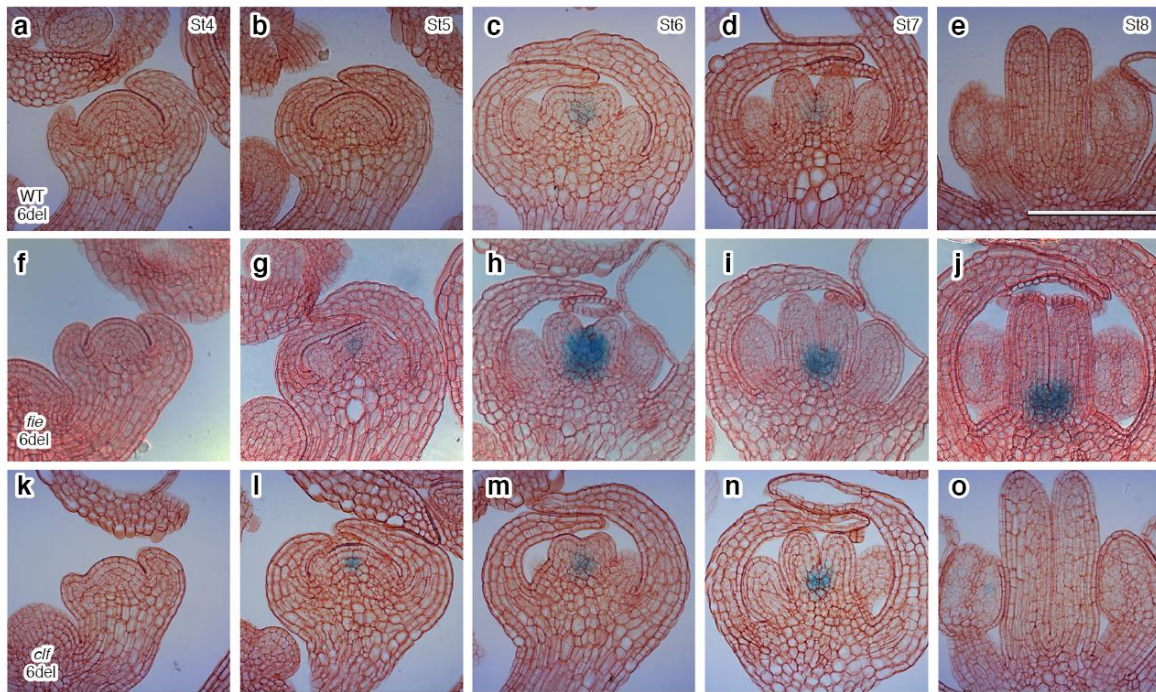
Fig. 22: *KNU-GUS* **stage specific expression pattern in** *6del* **and in** *6del* **in PRC2 mutant backgrounds.**

Representative longitudinal GUS sections from stage 4 to 8 of *6del* floral buds in WT (**a-e**), *fie* (**f-j**)*,* and *clf* (**k-o**). Cell walls were stained with neutral red dye. Scale bar = 50 µm.
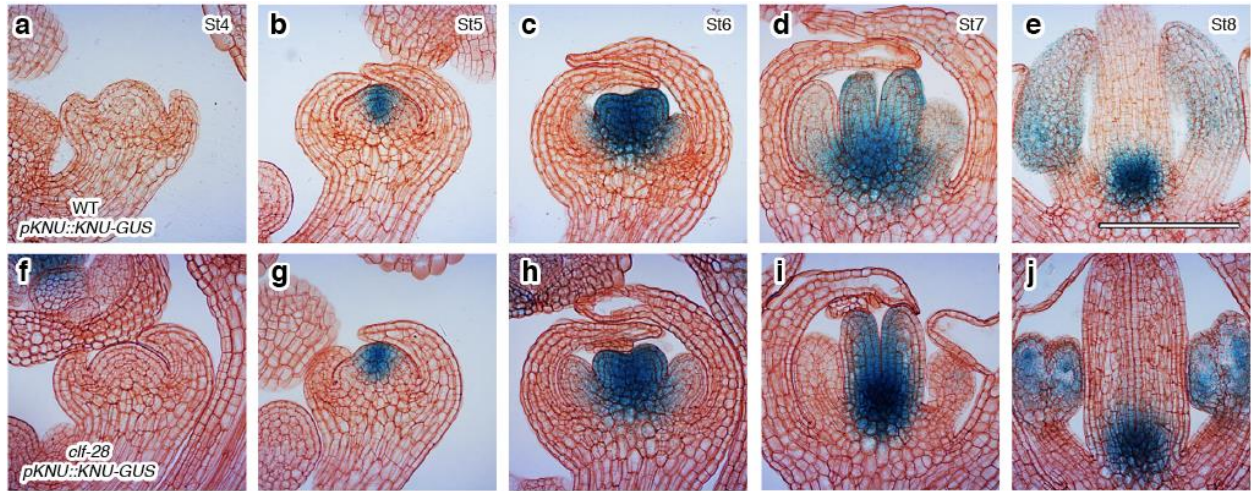
Fig. 23: *KNU* **stage-specific expression pattern in** *pKNU::KNU-GUS* **and** *pKNU::KNU-GUS* **in** *clf-28.*

Representative longitudinal GUS sections from stage 4 to 8 of *pKNU::KNU-GUS* floral buds in WT (**a-e**) and *clf-28* (**f-j**). Cell walls were stained with neutral red dye. Scale bar = 50 µm.
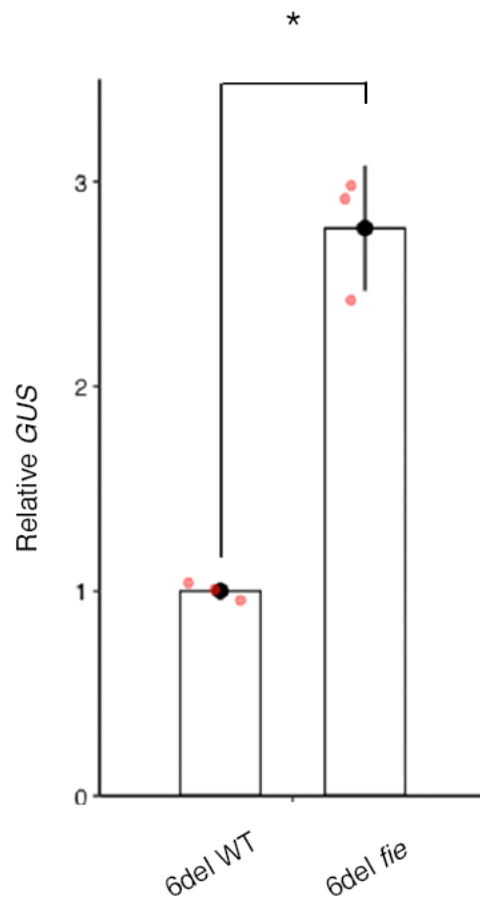
Fig. 24: *GUS* **transcript levels of** *6del* **in WT and** *fie* **determined by qRT-PCR.**

Data represent average fold changes ± standard errors of three biological replicates (n = 3). A two-tailed Student's *t*-test was used to determine significant differences ($p < 0.05$). *TUB2* served as the reference transcript.

Fig. 25: H3K27me3 enrichment in *6del* in WT compared to *fie* and *clf*.

Data represent average of % Input ± standard errors from three independent experiments (n = 3). A two-tailed Student's *t*-test was used to determine significant differences ($p < 0.05$). *EIF4A1* served as the negative control.

The cell cycle regulates H3K27me3 dilution on the extended *KNU* coding sequence

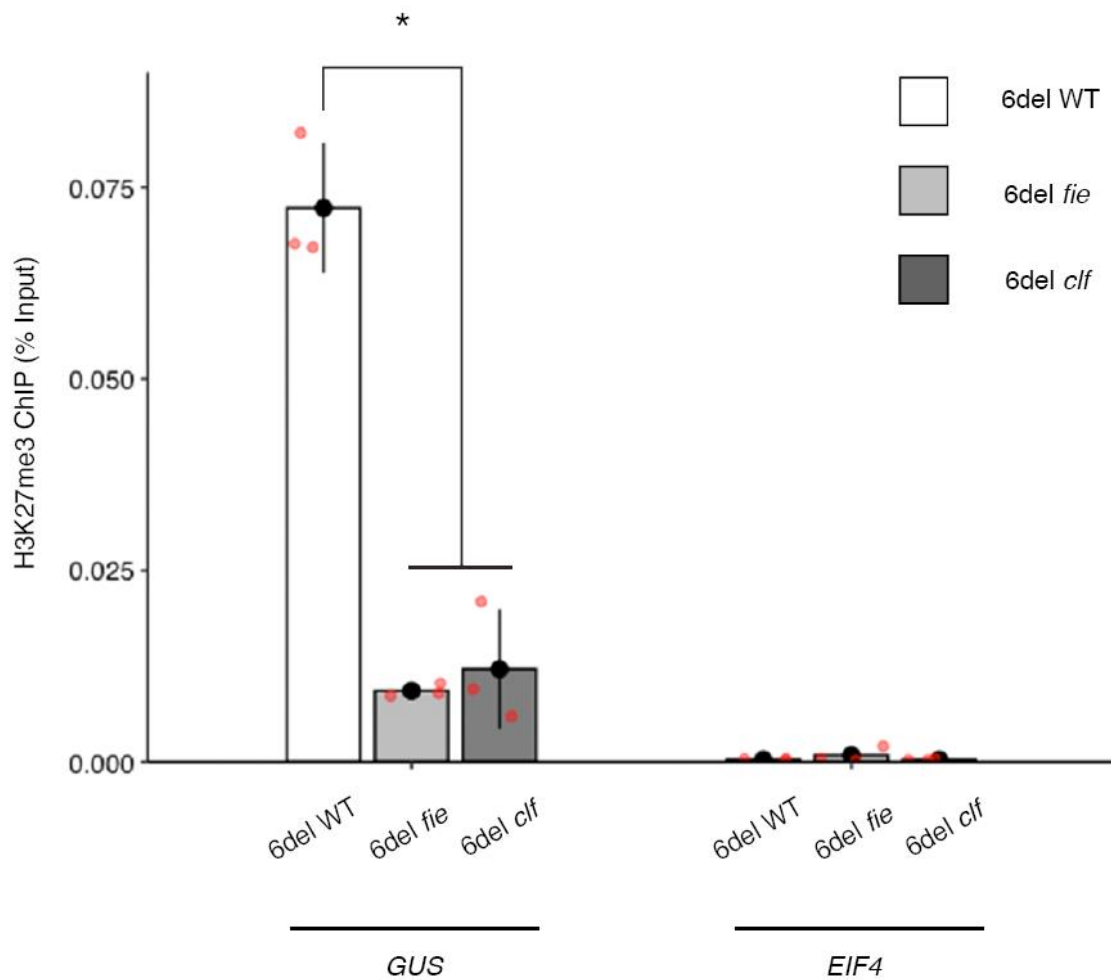The cell cycle plays an important role in *KNU* biotimer regulation by bringing about the dilution of H3K27me3 along the *KNU* coding sequence. To investigate whether mutations in cell cycle genes affect *del* regulation during *KNU* activation, *6del* was crossed into a quintuple *krp1 krp2 krp3 krp4 krp7* mutant (hereinafter referred to as *krp*)[59] (Fig. 26a-j). *krp* exhibits increased cell proliferation and leaf cell size likely as a result of enhanced CDK activity, which induces more phosphor-RBR1 and upregulation of the E2F pathway[59]. Similar to the PRC2 mutants, the *krp* mutant also showed precocious *6del* expression from stage 5 floral buds (Fig. 26f-j). In *krp*, *6del* expression peaked at stages 6 and 7 (Fig. 26h-i). These expression levels in *krp* were significantly increased compared to WT (Fig. 26a-e). Although only a faint signal was detected in *6del* in WT, *krp* mutants still possessed visible *6del* expression at stage 8 (Fig. 26e and j). Additionally, *GUS* transcript quantification in *krp* showed a significant increase in *6del* expression (Fig. 27). Correlated with this expression change, H3K27me3 levels on *del* in *krp* showed a significant decrease compared to that in WT (Fig. 28). These results suggest that enhancing cell cycle activity via downregulated CDK inhibition results in accelerated H3K27me3 dilution along *del*.

Tissue-specific expression was also observed for floral stages 4-8 in *6del* grown in lower temperature conditions at 18°C. *Arabidopsis* grows optimally in temperatures ranging from 12°C-27°C[60]. However, it is also known that they are highly sensitive to fluctuations in the ambient temperature range which

induce changes in the intracellular environment in response to these external cues[60,61]. Environmental changes leading to lower temperatures are typically associated with slowing down cellular processes including the cell cycle[60,61]. Transcript accumulation was examined for selected CDK/cyclin inhibitors (CKIs), namely *KRP1*, *KRP2*, *SMR1*, *SMR2*, and *SMR3*, in *6del* grown in 22℃ compared to *6del* grown in 18°C. It was found that CKIs are significantly upregulated in *6del* grown in 18°C relative to *6del* grown in 22°C suggesting that the cell cycle is inhibited as a result of growth at lower temperature conditions (Fig. 29). The stage-specific expression pattern was also observed for the core cell cycle gene and G2/M transition regulator CYCB1 fused to YFP grown in 22°C and 18°C (Fig. 30). A prevalent CYCB1-YFP expression in stages 4 and 6 for CYCB1-YFP plants grown in 22°C was observed compared to those grown in 18°C suggesting that cyclin activity is indeed inhibited by upregulated CKIs activity due to lower temperature conditions. Thus, growth at lower ambient temperature conditions at 18°C was chosen to investigate the effects of an inhibited cell cycle progression in *6del*.

For *6del* grown in 18°C, *KNU* expression was not evident from stages 4-6 and was observed only by stage 7 (Fig. 26k-n). By stage 8, *KNU* expression has attenuated and is unobservable (Fig. 26o). Meanwhile, apparent differences in *KNU* expression from stages 4-8 for *pKNU::KNU-GUS* grown in 22°C and 18°C were unobservable (Fig. 31). H3K27me3 levels were also significantly higher for *6del* at 18°C compared to *6del* at 22°C (Fig. 28). These results suggest that lower temperatures can further delay *KNU* activation in *6del* likely due to slower dilution of H3K27me3 along the extended region as intracellular activities also slow down which involves the cell cycle.
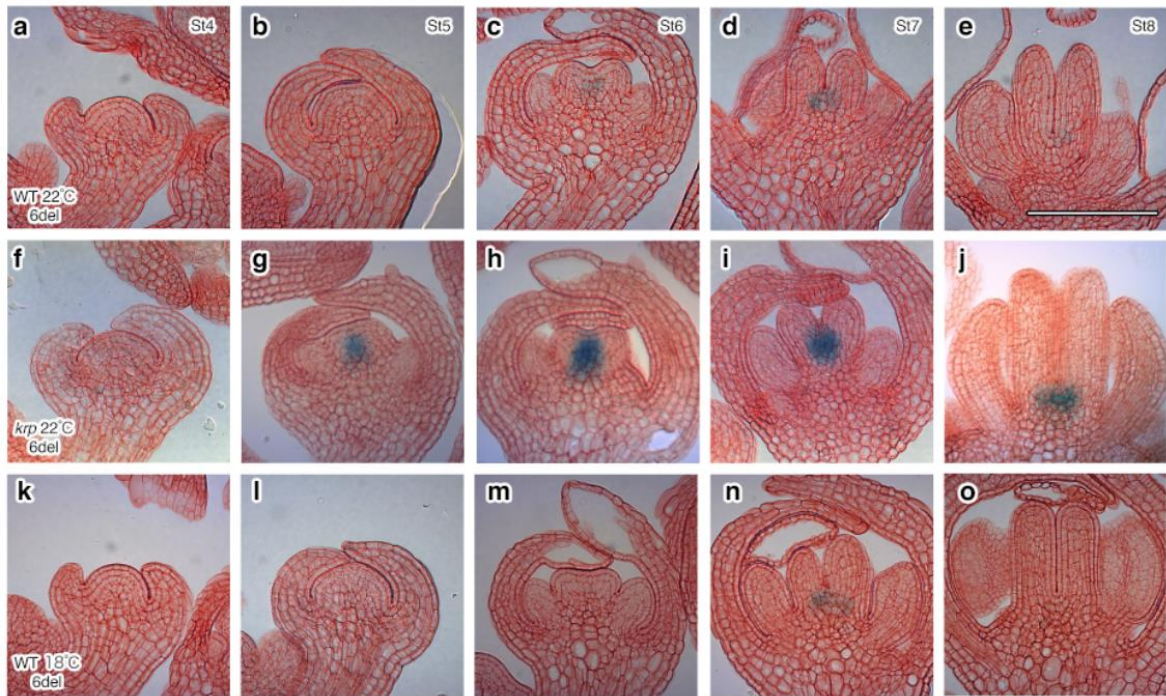
Fig. 26: *KNU-GUS* **stage specific expression pattern in** *6del* **and in** *6del krp* **grown at 22°C and in** *6del* **grown at 18°**C.

Representative longitudinal GUS sections from stage 4 to 8 floral buds of *6del* in WT (**a-e**), *6del krp* 22°C (**f-j**), and *6del* in WT 18°C (**k-o**). Cell walls were stained with neutral red dye. Scale bar = 50 μm.
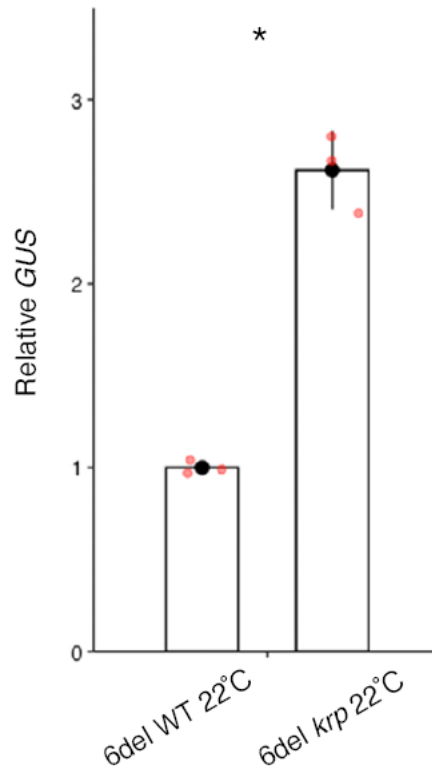
Fig. 27: *GUS* transcript levels of *6del* in WT and *6del krp* 22°C.

Transcript accumulation *6del* in WT and *6del krp* grown at 22°C was determined by qRT-PCR using RNA isolated from floral bud clusters containing flowers until stage 12. Data represent average fold changes ± standard errors of three biological replicates (n = 3). A two-tailed Student's *t*-test was used to determine significant differences ($p < 0.05$). *TUB2* served as the reference transcript.
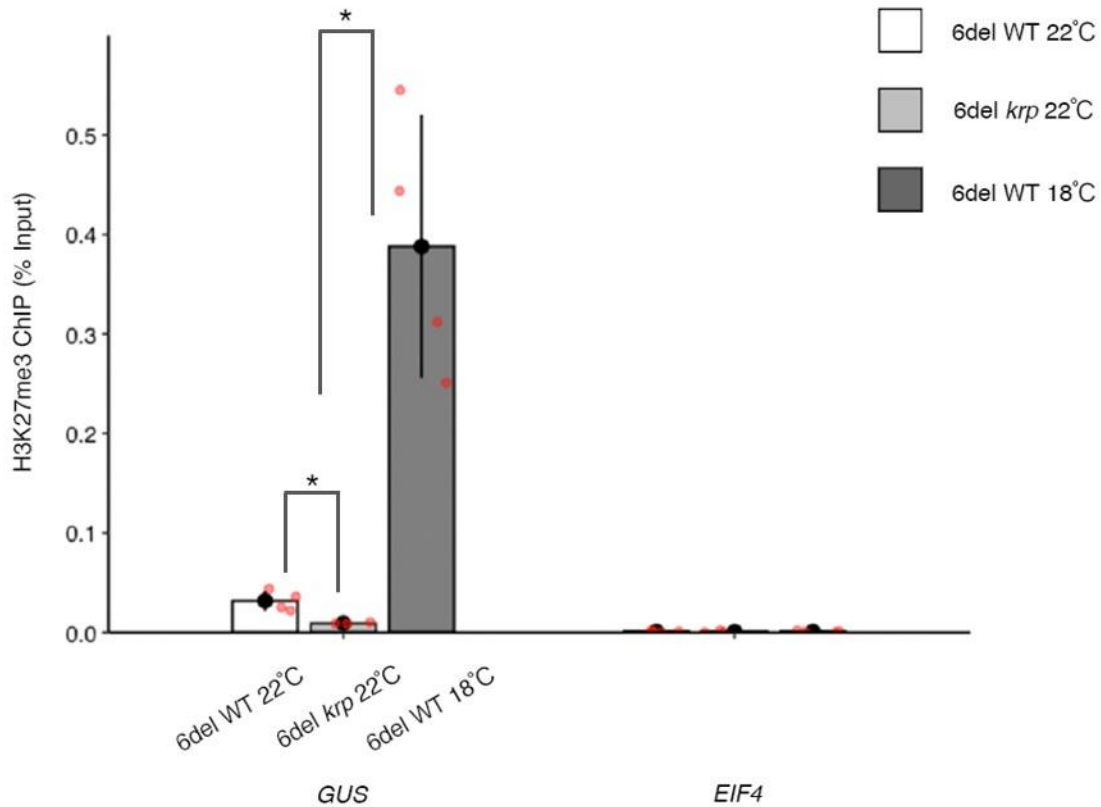
Fig. 28: H3K27me3 enrichment in *6del* in WT compared to *6del krp* 22°C and for *6del* in WT compared to *6del* in WT 18°C.

Samples used were floral bud clusters containing flowers until stage 12. Data represent average of % Input ± standard errors from four biological replicates (n = 4). A two-tailed Student's *t*-test was used to determine significant differences ($p < 0.05$). *EIF4A1* served as the negative control.
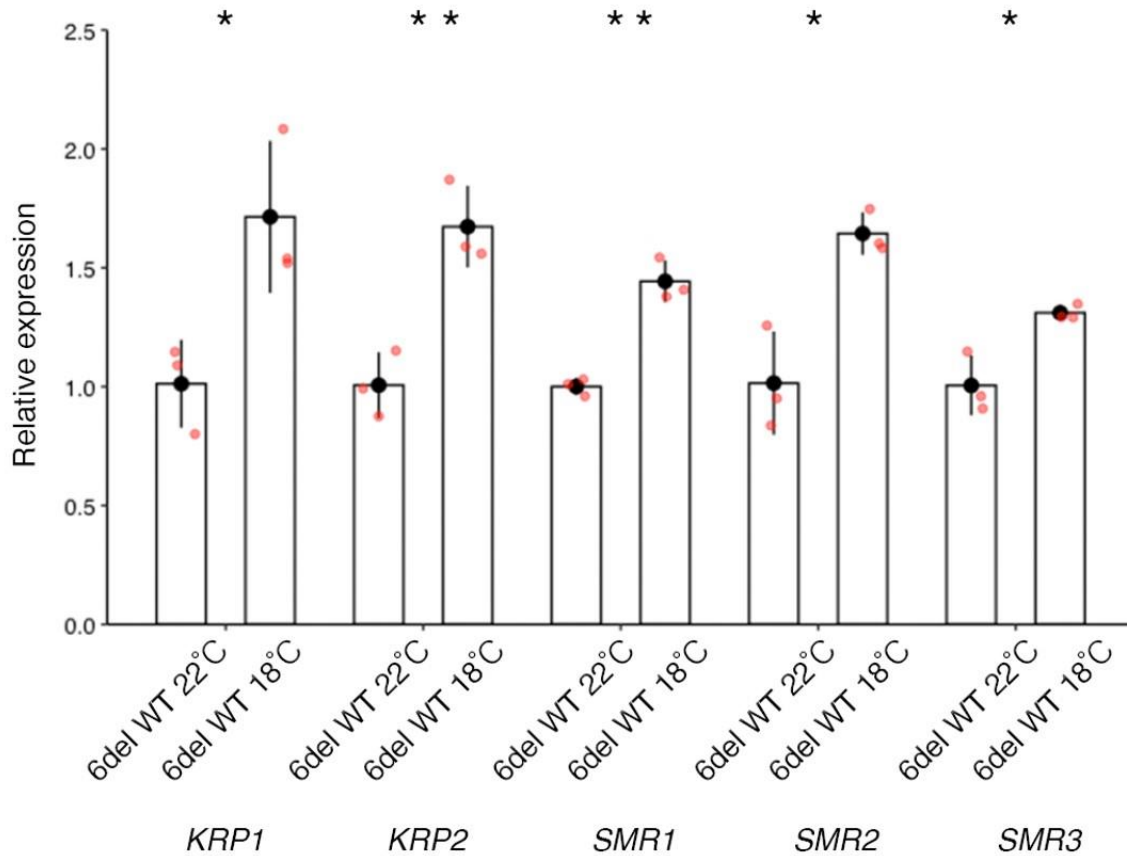
Fig. 29: Transcript levels of selected CKIs for *6del* WT grown in 22°C and 18°C determined by qRT-PCR.

RNA was isolated from floral bud clusters containing flowers until stage 12. Data represent average fold changes ± standard errors of three biological replicates (n = 3). A two-tailed Student's *t*-test was used to determine significant differences ($* = p < 0.05$, $** = p < 0.01$). *TUB2* served as the reference transcript.
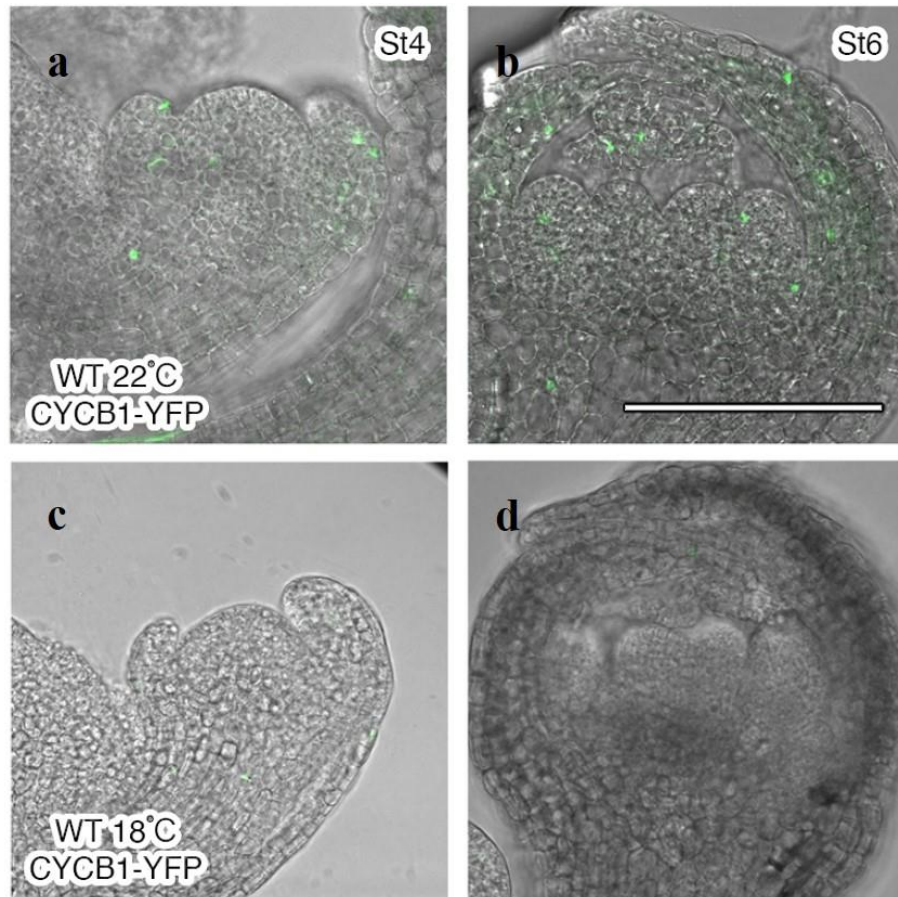
Fig. 30: CYCB1-YFP accumulation at floral stages 4 and 6 grown at 22°C and 18°C.

Representative longitudinal sections from stage 4 and 6 floral buds of CYCB1-YFP grown in 22°C (**a, b**) and in 18°C (**c, d**). Scale bar = 50 µm.
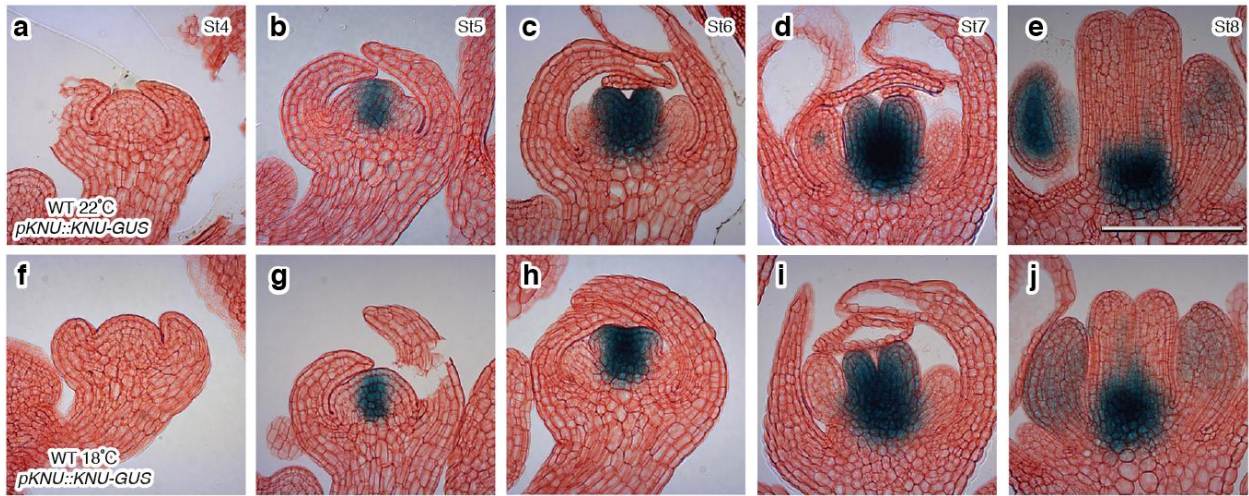
Fig. 31: Stage-specific *KNU* expression pattern in *pKNU::KNU-GUS* grown in 22°C and 18°C.

Representative longitudinal GUS sections from stage 4 to 8 of *pKNU::KNU-GUS* floral buds in WT grown at 22°C (**a-e**) and 18°C (**f-j**). Cell walls were stained with neutral red dye. Scale bar = 50 µm.

IV. Discussion

In this study, it was demonstrated that *KNU* is part of a biotimer gene regulatory network which integrates AG transcriptional signaling and H3K27me3 status. By analyzing relevant genome-wide *in silico* data, ten candidate biotimer genes (including *KNU*) that are regulated similarly as *KNU* were annotated. These genes are direct AG downstream targets, are highly enriched for H3K27me3 along the gene body, and show a delayed transcriptional activation upon AG binding associated with cell division cycles. These results suggest that this mode of transcriptional regulation may be recurring throughout flower development especially during floral meristem termination. Further analysis of these genes focused on the downregulated set at stages 6-7 relative to stages 3-4 in *ag ap1 cal::35SAG-GR* in which *KNU* also sorted into. Among these are members of well-characterized TF families, such as *STY1, AHL18* and *IDD12*, all of which are implicated in organ patterning and formation. For example, *STY1* is a known regulator of carpel development wherein it determines proper apical-basal patterning of the gynoecium by directly activating the auxin biosynthesis gene *YUCCA4* (*YUC4*)[19]. *STY1*, together with other *SHORT INTERNODES* (*SHI*)/*STY* genes, also plays a role in leaf vein and anther development, largely by regulating auxin biosynthesis and responses in these events, respectively[62,63]. Meanwhile, *AHL18* has recently been characterized as a regulator of lateral root development through a forward genetic screen using enhancer and gene trap lines[21]. In *Arabidopsis*, regulatory roles of various members of the *AHL* gene family are broad in scope[21]. *AHLs* have been implicated in the initiation of leaf senescence, hypocotyl elongation, hormone biosynthesis, as well as flowering time regulation [64–71]. *AHL21* or

GIANT KILLER, is a known regulator of proper reproductive organ specification during flower development that is directly under AG control[65]. *AHL*s are known for their multilevel modes of regulation, linking transcription factor activity with chromatin remodeling, and enabling the activation and repression of genes simultaneously[65,71]. Lastly, *IDD12* is a member of the INDETERMINATE DOMAIN (IDD) family of TFs which is involved in root formation via interaction with GRAS family TFs, namely SHORT ROOT (SHR) and SCARECROW (SCR)[20,72,73]. Other IDD proteins have also been implicated in GA synthesis by interacting with DELLA proteins[74]. Hence, the identification of *STY1*, *AHL18*, and *IDD12* as candidate biotimer genes suggests that various regulatory modules involving hormone pathways and chromatin remodeling are downstream of biotimer regulation. As *AHL18* and *IDD12* are members of TF families involved in root development, this may indicate that a wider set of genes may also be regulated by the biotimer mechanism and throughout other phases of plant development.

The mechanistic determinants of the biotimer and their interactions were investigated by chromatin manipulation of *KNU* with *del*, a region downstream of the *KNU* coding sequence that plays a role in *KNU* temporal regulation. Using a GUS reporter system, it was found that iterative addition of *del* in *KNU* results in progressive delay of *KNU* temporal activation as the number of *del* repeats increase. First, the WT *KNU* expression pattern was observed from stages 4-8 (Fig. 16a-e). AG activity begins at floral stage 3 wherein competitive binding with PRC2 at the *KNU* promoter region can be detected[14]. *KNU* is not yet expressed at stage 4 (Fig. 16c) suggesting that this corresponds to the observed time delay in *KNU* expression upon initial activation by AG. This also

suggests that PRC2 displacement at stage 3 leads to the subsequent decrease in H3K27me3 deposition at stage 4, as well as in its removal along the *KNU* coding sequence (CDS) upon cell division (Fig. 32a-b). The *KNU* CDS has a length of 451 bp. This is equivalent to approximately three nucleosomes made up of about 150-200 bp of DNA wrapped around the histone octamer and each marked with H3K27me3 (Fig. 32a). The *del* region downstream of *KNU* consists of 231 bp roughly corresponding to one nucleosome that is bound by FIE aside from the H3K27me3 mark (Fig. 32a). It may be that each cell division cycle from floral stage 3 results in the removal of H3K27me3 on a marked nucleosome at the *KNU* CDS. Hence, proliferating cells at stage 4 may be heterogenous for H3K27me3 bound at *KNU* wherein initial cells have one nucleosome without H3K27me3 and resulting progeny cells have two nucleosomes unmarked with H3K27me3. Another assumption is that the H3K27me3 marks diluted during cell division occurs from the *del* region because of *del*'s demonstrated role in regulating *KNU*'s temporal activation. Thus, by stage 5, H3K27me3 may be completely removed in some cells and the beginning of *KNU* expression is observed (Fig. 32c). *KNU* expression peaks at stage 6 as at this point, majority of proliferating cells are unmarked by H3K27me3 at the *KNU* CDS (Fig. 32d). Most importantly, this corresponds to the proper timing of floral meristem termination ensuring that the proper number of floral organs will develop. By stage 7, a reduction was observed in *KNU* expression and it can be speculated that PRC2 activity resumes at this stage (Fig. 32e). Perhaps an upstream regulator of AG also leads to a decrease in AG activity at the *KNU* promoter region allowing PRC2 activity to resume. This continues until stage 8 and whether *KNU* repression is also modulated by

the cell cycle, methylases or a combination of both remains to be demonstrated (Fig. 32f).

For *6del*, wherein six repeats of the *del* region were added to the *KNU* CDS (Fig. 33a), a prolonged delay in activating *KNU* expression was observed. *KNU* activation began at stage 6 in *6del* instead of stage 5 compared to the WT. These results suggest that the prolonged delay is due to the increased number of nucleosomes marked with H3K27me3 leading to only partial dilution by stage 5 (Fig. 33b-c). Following the proposed model, H3K27me3 removal is incomplete by stage 6 (Fig. 33d). The minimal *KNU* signal observed at this stage may be accounted for by a small pool of dividing cells wherein the H3K27me3 and FIE on the endogenous *del* has been removed. At stage 7, H3K27me3 removal may still be incomplete in dividing cells (Fig. 33e). Hence, although *KNU* expression in *6del* peaks at stage 7, it is markedly reduced compared to the WT's peak *KNU* expression at stage 6. *KNU* repression by stage 7 may also contribute to this reduction. By stage 8, *KNU* expression is unobservable suggesting that the additional *del* regions augment *KNU* repression via H3K27me3 deposition (Fig. 33f). *6del* in the FIE co-suppression background suggests that H3K27me3 deposition on the extended region is modulated by PRC2 based on the earlier and stronger *KNU* induction in *6del fie*. This indicates that an intact PRC2 machinery is necessary for proper *KNU* temporal activation by modulating H3K27me3 deposition and maintenance along the *KNU* gene body. Disrupting the PRC2 machinery is sufficient to modify *KNU*'s temporal activation in *6del* as observed in both *6del fie* and *6del clf*.

As H3K27me3 removal along *KNU* is cell division-dependent, the results for *6del* also suggest that more cell cycles are needed to dilute H3K27me3 along the extended region completely, and contributes to the delay and reduction observed in *KNU* expression. Thus, *6del krp* was generated to understand how the cell cycle modulates *KNU*'s biotimer regulation. An earlier and stronger *KNU* induction in *6del krp* was observed indicating that proper cell cycle progression is necessary for *KNU*'s temporal activation in *6del* by facilitating H3K27me3 removal. Meanwhile, *KNU* activation for *6del* grown in 18°C was also delayed likely due to prolonged cell cycle duration as a result of intrinsic responses in response to growth in lower ambient temperature conditions. This emphasizes the dynamic regulation of H3K27me3 in response to extracellular and intracellular cues and suggests the role of the cell cycle-dependent biotimer in coordinating the balance between cell proliferation and differentiation under ever-changing conditions. Additional experiments to demonstrate whether low temperature stress networks are activated upon growth at 18°C will be necessary to clarify the effect of lower temperature conditions on the cell cycle and on biotimer regulation. Primarily, these results indicate that the number and duration of cell cycles play a major role in *KNU*'s proper temporal regulation in *6del* and demonstrates how the cell cycle may be able to coordinate differentiation speed with termination timing of stem cell activities.

Overall, these findings highlight the complex and dynamic nature of H3K27me3 regulation for transcriptional activation in the context of floral meristem termination during flower development. In this study, novel candidate biotimer genes were annotated and a mechanistic perspective of the biotimer regulation modulated by PRC2 activity, chromatin environment, and the cell

cycle was provided. Future work will focus on demonstrating the biotimer regulation of the annotated candidate genes through further time-course analysis of gene expression and PRC2 binding at target loci, as well as the effect of cell cycle modulation through exogenous application of cell cycle accelerators and inhibitors. Specifically, the role of gene or coding sequence length marked with H3K27me3 in relation to the duration of temporal delay observed from the time of AG binding at target promoter regions will be addressed. Thus, the biotimer mechanism can be endogenously demonstrated in parallel with the *del* series which serves as a synthetic system. How many cell cycles are needed in *6del* until *KNU* is activated by working with additional cell cycle mutants will also be investigated, as well as identifying which specific phase of the cell cycle is crucial for *KNU* temporal activation. Finally, additional factors contributing to the observed reduction in *KNU* expression in the *del* variants by looking at transcriptional silencing activity will also be examined.
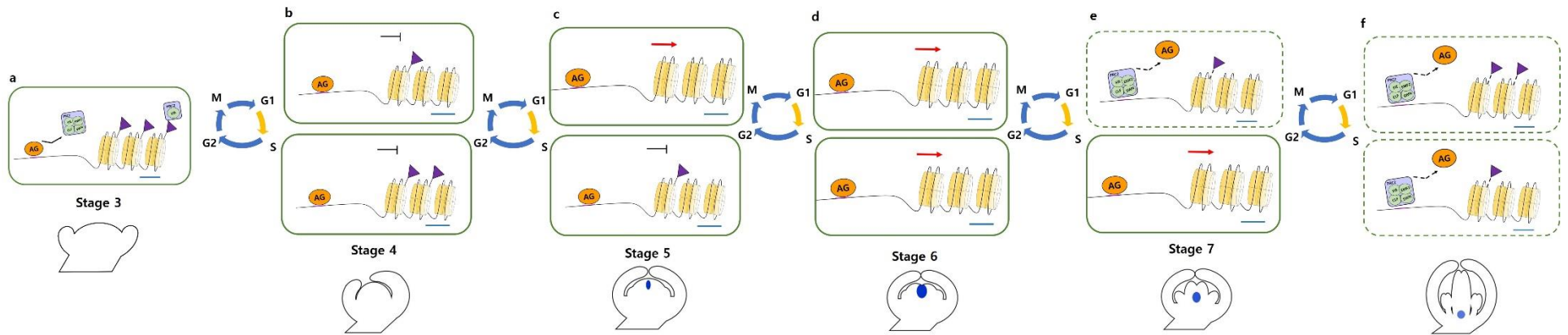
Fig. 32: Proposed model for *KNU* biotimer regulation in WT.

(**a**) AG expression at stage 3 leads to PRC2 displacement at the *KNU* promoter region. Events are depicted as occurring in cells (green rectangle). Yellow structures (histones) wrapped by thin black lines (DNA) represent nucleosomes. H3K27me3 is depicted as the violet triangle attached on each nucleosome. The three H3K27me3-marked nucleosomes represent the *KNU* coding sequence. The *del* region is indicated by the blue bar underneath the third nucleosome on which FIE binding is also illustrated. AG (round orange structure) and PRC2 (square light purple and green structure) are localized upstream of the *KNU* gene body. Cell division cycles are represented as events which precede stages 4-8 (blue and yellow arrows). Each cell cycle phase is indicated. The G1/S phase is highlighted by a yellow arrow representing the phase regulated by KRP.

(**b**) Cell cycle-dependent H3K27me3 dilution proceeds at the *KNU* CDS by stage 4 but is still incomplete. *KNU* remains repressed (represented by blunt black arrow above the *KNU* CDS).

(**c**) H3K27me3 dilution is complete for some cells and *KNU* activation is observed (represented by pointed red arrow above the *KNU* CDS).

(**d**) Majority of proliferating cells are H3K27me3-free at the *KNU* CDS by stage 6 and strong *KNU* induction is observed.

(**e**) *KNU* expression decreases by stage 7. Events depicted by dashed lines are speculative.

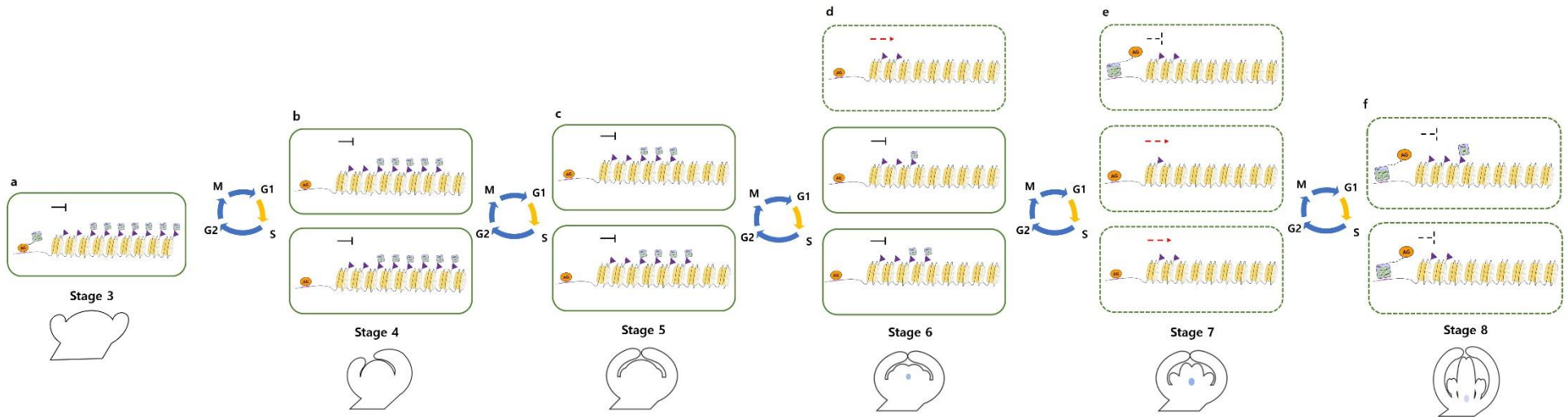(**f**) *KNU* expression further decreases by stage 8.

Fig. 33: Proposed model for *KNU* biotimer regulation in *6del*.

(**a**) The *KNU* CDS is extended with six additional *del* regions in *6del* (equivalent to 7 *del* regions including the endogenous *del*).

(**b**) Cell cycle-mediated H3K27me3 dilution proceeds from stage 3 to 4.

(**c**) At stage 5, H3K27me3 dilution is incomplete and *KNU* expression is not observed in *6del*.

(**d**) A minimal *KNU* signal is observed at stage 6. Presumably, there are cells that are free of the H3K27me3 mark on the *del* regions leading to *KNU* activation (represented by the dashed line cell). However, H3K27me3 dilution in most cells is still incomplete. Events depicted as dashed lines are speculative.

(**e**) *KNU* expression peaks at stage 7 in *6del* but considerably less than in the WT peak stage (stage 6). It is expected that this is due to incomplete dilution of H3K27me3 at the extended region (although most marks may have been removed on most of the *del* regions) and is also a result of the resumption of *KNU* repression.

(**f**) Little to no *KNU* expression is observed at stage 8 in *6del* suggesting that the extended region also contributes to the timing and degree of *KNU* repression at this stage.

References

1. Sablowski, R. Flowering and determinacy in Arabidopsis. *J Exp Bot* **58**, 899–907 (2007).

2. Liu, X. *et al.* AGAMOUS Terminates Floral Stem Cell Maintenance in Arabidopsis by Directly Repressing WUSCHEL through Recruitment of Polycomb Group Proteins. *The Plant Cell* **23**, 3654–3670 (2011).

3. Shang, E., Ito, T. & Sun, B. Control of floral stem cell activity in Arabidopsis. *Plant Signal Behav* **14**, (2019).

4. Xu, Y., Yamaguchi, N., Gan, E.-S. & Ito, T. When to stop: an update on molecular mechanisms of floral meristem termination. *J Exp Bot* **70**, 1711–1718 (2019).

5. Sun, B. & Ito, T. Regulation of floral stem cell termination in Arabidopsis. *Front Plant Sci* **6**, (2015).

6. Yanofsky, M. F. *et al.* The protein encoded by the Arabidopsis homeotic gene agamous resembles transcription factors. *Nature* **346**, 35–39 (1990).

7. Mayer, K. F. X. *et al.* Role of WUSCHEL in Regulating Stem Cell Fate in the Arabidopsis Shoot Meristem. *Cell* **95**, 805–815 (1998).

8. Lohmann, J. U. *et al.* A Molecular Link between Stem Cell Regulation and Floral Patterning in Arabidopsis. *Cell* **105**, 793–803 (2001).

9. Lenhard, M., Bohnert, A., Jürgens, G. & Laux, T. Termination of Stem Cell Maintenance in Arabidopsis Floral Meristems by Interactions between WUSCHEL and AGAMOUS. *Cell* **105**, 805–814 (2001).

10. Yamaguchi, N., Huang, J., Xu, Y., Tanoi, K. & Ito, T. Fine-tuning of auxin homeostasis governs the transition from floral stem cell maintenance to gynoecium formation. *Nat Commun* **8**, 1125 (2017).

11. Yamaguchi, N. *et al.* Chromatin-mediated feed-forward auxin biosynthesis in floral meristem determinacy. *Nat Commun* **9**, 5290 (2018).

12. Payne, T., Johnson, S. D. & Koltunow, A. M. KNUCKLES (KNU) encodes a C2H2 zinc-finger protein that regulates development of basal pattern elements of the Arabidopsis gynoecium. *Development* **131**, 3737–3749 (2004).

13. Sun, B., Xu, Y., Ng, K.-H. & Ito, T. A timing mechanism for stem cell maintenance and differentiation in the Arabidopsis floral meristem. *Genes Dev* **23**, 1791–1804 (2009).

14. Sun, B. *et al.* Timing Mechanism Dependent on Cell Division Is Invoked by Polycomb Eviction in Plant Stem Cells. *Science* **343**, (2014).

15. Bollier, N. *et al.* At-MINI ZINC FINGER2 and Sl-INHIBITOR OF MERISTEM ACTIVITY, a Conserved Missing Link in the Regulation of

Floral Meristem Termination in Arabidopsis and Tomato. *The Plant Cell* **30**, 83–100 (2018).

16. Sun, B. *et al.* Integration of Transcriptional Repression and Polycomb-Mediated Silencing of WUSCHEL in Floral Meristems. *The Plant Cell* **31**, 1488–1505 (2019).

17. Ikeuchi, M., Iwase, A. & Sugimoto, K. Control of plant cell differentiation by histone modification and DNA methylation. *Current Opinion in Plant Biology* **28**, 60–67 (2015).

18. Ó'Maoiléidigh, D. S. *et al.* Control of Reproductive Floral Organ Identity Specification in Arabidopsis by the C Function Regulator AGAMOUS. *The Plant Cell* **25**, 2482–2503 (2013).

19. Sohlberg, J. J. *et al.* STY1 regulates auxin homeostasis and affects apical–basal patterning of the Arabidopsis gynoecium. *The Plant Journal* **47**, 112–123 (2006).

20. Aoyanagi, T., Ikeya, S., Kobayashi, A. & Kozaki, A. Gene Regulation via the Combination of Transcription Factors in the INDETERMINATE DOMAIN and GRAS Families. *Genes* **11**, 613 (2020).

21. Širl, M. *et al.* At-Hook Motif Nuclear Localised Protein 18 as a Novel Modulator of Root System Architecture. *International Journal of Molecular Sciences* **21**, 1886 (2020).

22. Nagano, Y., Furuhashi, H., Inaba, T. & Sasaki, Y. A novel class of plant-specific zinc-dependent DNA-binding protein that binds to A/T-rich DNA sequences. *Nucleic Acids Research* **29**, 4097–4105 (2001).

23. Xiao, J. *et al.* Cis and trans determinants of epigenetic silencing by Polycomb repressive complex 2 in Arabidopsis. *Nature Genetics* **49**, 1546–1552 (2017).

24. Yoon, K.-J., Vissers, C., Ming, G. & Song, H. Epigenetics and epitranscriptomics in temporal patterning of cortical neural progenitor competence. *J Cell Biol* **217**, 1901–1914 (2018).

25. Eccleston, A., Cesari, F. & Skipper, M. Transcription and epigenetics. *Nature* **502**, 461–461 (2013).

26. Mozgova, I., Köhler, C. & Hennig, L. Keeping the gate closed: functions of the polycomb repressive complex PRC2 in development. *The Plant Journal* **83**, 121–132 (2015).

27. Bemer, M. & Grossniklaus, U. Dynamic regulation of Polycomb group activity during plant development. *Current Opinion in Plant Biology* **15**, 523–529 (2012).

28. Mozgova, I. & Hennig, L. The Polycomb Group Protein Regulatory Network. *Annu. Rev. Plant Biol.* **66**, 269–296 (2015).

29. Kim, D.-H. & Sung, S. Polycomb-Mediated Gene Silencing in Arabidopsis thaliana. *Mol Cells* **37**, 841–850 (2014).

30. Ramachandran, S. & Henikoff, S. Replicating nucleosomes. *Science Advances* **1**, e1500587 (2015).

31. Alabert, C. *et al.* Two distinct modes for propagation of histone PTMs across the cell cycle. *Genes Dev.* **29**, 585–590 (2015).

32. Lai, W. K. M. & Pugh, B. F. Understanding nucleosome dynamics and their links to gene expression and DNA replication. *Nature Reviews Molecular Cell Biology* **18**, 548–562 (2017).

33. Bogliotti, Y. S. & Ross, P. J. Mechanisms of histone H3 lysine 27 trimethylation remodeling during early mammalian development. *Epigenetics* **7**, 976–981 (2012).

34. Zik, M. & Irish, V. F. Flower Development: Initiation, Differentiation, and Diversification. *Annu. Rev. Cell Dev. Biol.* **19**, 119–140 (2003).

35. Mambro, R. D. *et al.* Auxin minimum triggers the developmental switch from cell division to cell differentiation in the Arabidopsis root. *PNAS* **114**, E7641–E7649 (2017).

36. Harashima, H. & Sekine, M. Cyclin-Dependent Protein Kinases in the Control of Cell Cycle in Plants. in *Protein Kinases and Stress Signaling in Plants* 347–368 (John Wiley & Sons, Ltd, 2020). doi:10.1002/9781119541578.ch14.

37. Kumar, N. & Larkin, J. C. Why do plants need so many cyclin-dependent kinase inhibitors? *Plant Signaling & Behavior* **12**, e1282021 (2017).

38. Veylder, L. D. *et al.* Functional Analysis of Cyclin-Dependent Kinase Inhibitors of Arabidopsis. *The Plant Cell* **13**, 1653–1668 (2001).

39. Churchman, M. L. *et al.* SIAMESE, a Plant-Specific Cell Cycle Regulator, Controls Endoreplication Onset in Arabidopsis thaliana. *Plant Cell* **18**, 3145–3157 (2006).

40. Thorvaldsdóttir, H., Robinson, J. T. & Mesirov, J. P. Integrative Genomics Viewer (IGV): high-performance genomics data visualization and exploration. *Brief Bioinform* **14**, 178–192 (2013).

41. Chen, L., Wang, F., Wang, X. & Liu, Y.-G. Robust one-Tube Ω-PCR Strategy Accelerates Precise Sequence Modification of Plasmids for Functional Genomics. *Plant Cell Physiol* **54**, 634–642 (2013).

42. Weigel, D. & Glazebrook, J. *Arabidopsis: A Laboratory Manual*. (CSHL Press, 2002).

43. Yamaguchi, N. *et al.* PROTOCOLS: Chromatin Immunoprecipitation from Arabidopsis Tissues. *Arabidopsis Book* **12**, (2014).

44. Ito, T. *et al.* The homeotic protein AGAMOUS controls microsporogenesis by regulation of SPOROCYTELESS. *Nature* **430**, 356–360 (2004).

45. Gómez-Mena, C., Folter, S. de, Costa, M. M. R., Angenent, G. C. & Sablowski, R. Transcriptional program controlled by the floral homeotic gene AGAMOUS during early organogenesis. *Development* **132**, 429–438 (2005).

46. Barton, M. K. & Poethig, R. S. Formation of the shoot apical meristem in Arabidopsis thaliana: an analysis of development in the wild type and in the shoot meristemless mutant. *Development* **119**, 823–831 (1993).

47. Han, G. *et al.* Arabidopsis ZINC FINGER PROTEIN1 Acts Downstream of GL2 to Repress Root Hair Initiation and Elongation by Directly Suppressing bHLH Genes. *The Plant Cell* **32**, 206–225 (2020).

48. Bosco, C. D. *et al.* Inactivation of the Chloroplast ATP Synthase γ Subunit Results in High Non-photochemical Fluorescence Quenching and Altered Nuclear Gene Expression in Arabidopsis thaliana. *J. Biol. Chem.* **279**, 1060–1069 (2004).

49. Hanada, K. *et al.* Functional Compensation of Primary and Secondary Metabolites by Duplicate Genes in Arabidopsis thaliana. *Mol Biol Evol* **28**, 377–382 (2011).

50. Ma, C., Haslbeck, M., Babujee, L., Jahn, O. & Reumann, S. Identification and Characterization of a Stress-Inducible and a Constitutive Small Heat-Shock Protein Targeted to the Matrix of Plant Peroxisomes. *Plant Physiology* **141**, 47–60 (2006).

51. Riechmann, J. L. *et al.* Arabidopsis Transcription Factors: Genome-Wide Comparative Analysis Among Eukaryotes. *Science* **290**, 2105–2110 (2000).

52. Liu, S. *et al.* PLATZ2 negatively regulates salt tolerance in Arabidopsis seedlings by directly suppressing the expression of the CBL4/SOS3 and CBL10/SCaBP8 genes. *J Exp Bot* **71**, 5589–5602 (2020).

53. Gong, W. *et al.* Genome-Wide ORFeome Cloning and Analysis of Arabidopsis Transcription Factor Genes. *Plant Physiology* **135**, 773–782 (2004).

54. Tian, T. *et al.* agriGO v2.0: a GO analysis toolkit for the agricultural community, 2017 update. *Nucleic Acids Res* **45**, W122–W129 (2017).

55. Supek, F., Bošnjak, M., Škunca, N. & Šmuc, T. REVIGO Summarizes and Visualizes Long Lists of Gene Ontology Terms. *PLOS ONE* **6**, e21800 (2011).

56. Katz, A., Oliva, M., Mosquna, A., Hakim, O. & Ohad, N. FIE and CURLY LEAF polycomb proteins interact in the regulation of homeobox gene expression during sporophyte development. *The Plant Journal* **37**, 707–719 (2004).

57. Doyle, M. R. & Amasino, R. M. A Single Amino Acid Change in the Enhancer of Zeste Ortholog CURLY LEAF Results in Vernalization-Independent, Rapid Flowering in Arabidopsis. *Plant Physiology* **151**, 1688–1697 (2009).

58. Liu, J. *et al.* CURLY LEAF Regulates Gene Sets Coordinating Seed Size and Lipid Biosynthesis. *Plant Physiology* **171**, 424–436 (2016).

59. Cheng, Y. *et al.* Downregulation of multiple CDK inhibitor ICK/KRP genes upregulates the E2F pathway and increases cell proliferation, and organ and seed sizes in Arabidopsis. *The Plant Journal* **75**, 642–655 (2013).

60. Wigge, P. A. Ambient temperature signalling in plants. *Current Opinion in Plant Biology* **16**, 661–666 (2013).

61. Michael, T. P. *et al.* Network Discovery Pipeline Elucidates Conserved Time-of-Day–Specific cis-Regulatory Modules. *PLOS Genetics* **4**, e14 (2008).

62. Baylis, T., Cierlik, I., Sundberg, E. & Mattsson, J. SHORT INTERNODES/STYLISH genes, regulators of auxin biosynthesis, are involved in leaf vein development in Arabidopsis thaliana. *New Phytologist* **197**, 737–750 (2013).

63. Estornell, L. H., Landberg, K., Cierlik, I. & Sundberg, E. SHI/STY Genes Affect Pre- and Post-meiotic Anther Processes in Auxin Sensing Domains in Arabidopsis. *Front. Plant Sci.* **9**, (2018).

64. Wong, M. M. *et al.* Phosphoproteomics of Arabidopsis Highly ABA-Induced1 identifies AT-Hook–Like10 phosphorylation required for stress growth regulation. *PNAS* **116**, 2354–2363 (2019).

65. Ng, K.-H., Yu, H. & Ito, T. AGAMOUS Controls GIANT KILLER, a Multifunctional Chromatin Modifier in Reproductive Organ Patterning and Differentiation. *PLOS Biology* **7**, e1000251 (2009).

66. Lim, P. O. *et al.* Overexpression of a chromatin architecture-controlling AT-hook protein extends leaf longevity and increases the post-harvest storage life of plants. *The Plant Journal* **52**, 1140–1153 (2007).

67. Yadeta, K. A. *et al.* The Arabidopsis thaliana DNA-Binding Protein AHL19 Mediates Verticillium Wilt Resistance. *MPMI* **24**, 1582–1591 (2011).

68. Matsushita, A., Furumoto, T., Ishida, S. & Takahashi, Y. AGF1, an AT-Hook Protein, Is Necessary for the Negative Feedback of AtGA3ox1 Encoding GA 3-Oxidase. *Plant Physiol* **143**, 1152–1162 (2007).

69. Lee, K. & Seo, P. J. Coordination of matrix attachment and ATP-dependent chromatin remodeling regulate auxin biosynthesis and Arabidopsis hypocotyl elongation. *PLOS ONE* **12**, e0181804 (2017).

70. Street, I. H., Shah, P. K., Smith, A. M., Avery, N. & Neff, M. M. The AT-hook-containing proteins SOB3/AHL29 and ESC/AHL27 are negative modulators of hypocotyl growth in Arabidopsis. *The Plant Journal* **54**, 1–14 (2008).

71. Zhou, J., Wang, X., Lee, J.-Y. & Lee, J.-Y. Cell-to-Cell Movement of Two Interacting AT-Hook Factors in Arabidopsis Root Vascular Tissue Patterning. *The Plant Cell* **25**, 187–201 (2013).

72. Laurenzio, L. D. *et al.* The SCARECROW Gene Regulates an Asymmetric Cell Division That Is Essential for Generating the Radial Organization of the Arabidopsis Root. *Cell* **86**, 423–433 (1996).

73. Lucas, M. *et al.* SHORT-ROOT Regulates Primary, Lateral, and Adventitious Root Development in Arabidopsis. *Plant Physiology* **155**, 384–398 (2011).

74. Fukazawa, J. *et al.* DELLAs Function as Coactivators of GAI-ASSOCIATED FACTOR1 in Regulation of Gibberellin Homeostasis and Signaling in Arabidopsis. *The Plant Cell* **26**, 2920–2938 (2014).